Mode Selection Rules and Bifurcation Diagrams for Two-Delay Systems: Underlying Mechanism Controlled by Embedded Multidimensional Maps

doi: info:doi/10.7566/JPSJ.88.024002

Mode Selection Rules and Bifurcation Diagrams for Two-Delay Systems: Underlying Mechanism Controlled by Embedded Multidimensional Maps

Kin'ya Takahashi[1]* and Taizo Kobayashi[2,3]

[1] *Department of Physics and Information Engineering, Kyushu Institute of Technology, Kawazu 680-4, Iizuka 820-8502, Japan*

[2]*Faculty of Fukuoka Medical Technology, Teikyo University, 6-22 Misaki-machi, Omuta, 836-8505, Japan*

[3]*Research Institute for Information Technology, Kyushu University, 744 Motooka, Nishi-ku, Fukuoka 819-0395, Japan*

We study mode selection rules at the first bifurcation and bifurcation diagrams for a two-delay system with a positive feedback of a long delay time t_2 and with either a positive or negative feedback of a short delay time t_1, i.e., $0 < t_1 < t_2$. The mode excited by the first bifurcation changes with t_1/t_2, and the relevant and irrelevant conditions, which are rational numbers in t_1/t_2 with $t_1/t_2 = n/m$, characterize the mode selection rule; a definite subset of the rational numbers is relevant and its complement is irrelevant. In a neighborhood of a relevant condition, oscillations each with period $T \approx 2t_2/m$, i.e., mth-order harmonic, are excited at the first bifurcation. In a neighborhood of an irrelevant condition, twin peaks consisting of higher-order harmonics are observed. The mode selection rule markedly changes with the strength of the short delay; the relevant condition changes reflecting the change in the underlying mechanism of the bifurcation process. In this paper, we show that for each of the relevant and irrelevant conditions, the two-delay system is reduced to an m-dimensional map in the nondispersive limit, i.e., a singular perturbation limit. In terms of multidimensional maps, the first bifurcation for the relevant condition is either a pitchfork or period-doubling bifurcation, while a Hopf bifurcation is observed for the irrelevant condition. The mode selection rules together with the waveforms are explained from the analysis of the multidimensional maps. Furthermore, the global structure of transitions among attractors after the first bifurcation is approximately predicted from the analysis of the multidimensional maps.

1. Introduction

In the last half century, time-delay systems have attracted many authors' attention in the fields of physics, chemistry, biology, acoustics, engineering, economics, and so forth.[1–5] Two-delay and multiple-delay systems have been studied in a wide range of research areas from pure mathematics to practical applications.[6–20] For example, multiple-delay systems can be applied to the study of the sounding mechanism of woodwind musical instruments with tone holes, e.g., the clarinet.[18,21–23] In a previous work, we have shown that the function of the register hole of the clarinet is well explained by the characteristics of two-delay systems.[18] From the viewpoints of nonlinear physics and mathematics, time-delay systems are multiattractor systems. As the control parameter μ is varied from a static solution in a weak nonlinear regime, one of the attractors is selected by the first bifurcation, normally a Hopf bifurcation, which generates an oscillation on the selected attractor. Thus, the problem as to which oscillation mode among many attractors is selected by the first bifurcation is crucial for the study of multiple-delay systems.[6–9,18–20] To the best of the authors' knowledge, the mode selection rules for multiple-delay systems are not yet understood in detail.[6–20]

For two-delay systems, the mode excited by the first bifurcation sensitively changes with the ratio of delay times t_1/t_2, where t_1 and t_2 are short and long delay times, respectively, with $0 < t_1 \leq t_2$ and t_2 fixed.[6–9,18,20] In the analysis of mode selection rules, the notion of relevant and irrelevant conditions is important. Roughly speaking, the relevant and irrelevant conditions are rational numbers in t_1/t_2 with $t_1/t_2 = n/m$ (for details, see Sect. 2).[6,9,18,20] In a neighborhood of a relevant condition, oscillations each with period $T \approx 2t_2/m$, i.e., the mth-order harmonic, are excited at the first bifurcation. In a neighborhood of an irrelevant condition, twin peaks consisting of higher-order harmonics, called the tower structure, are observed, although a lower-order harmonic is observed at the center of the tower structure.[6] For two-delay systems with two positive feedback loops, the relevant condition is given as t_1/t_2 =odd/odd, while the conditions t_1/t_2 =even/odd and odd/even are irrelevant.

The two-delay system treated in this paper includes a nonlinear function $f(x)$, and the first bifurcation of the map $x_i = \mu(\alpha_1 + \alpha_2)f(x_{i-1})$ seems to trigger a Hopf bifurcation for the two-delay system,[6,9,18] where α_1 and α_2 are the strengths of short and long delays, respectively. For the two-delay system with two positive delay feedback loops, the period-doubling bifurcation of the map triggers the first bifurcation and the mode selection rule is governed by this mechanism of the first bifurcation. Let us call this bifurcation process the normal bifurcation process (NBP).[20] In a previous work,[20] we studied the two-delay system with positive and

*takahasi@mse.kyutech.ac.jp

negative feedback loops, i.e., a long delay of positive strength $\alpha_2 > 0$ and a short delay of negative strength α_1 in the range $-\alpha_2 < \alpha_1 < 0$, and found two mode selection rules different from that governed by NBP. In the range $\alpha_{th} < \alpha_1 < 0$, where $\alpha_{th}(> -\alpha_2)$ is a threshold value, the relevant condition is given as t_1/t_2 =even/odd, and t_1/t_2 =odd/odd and odd/even are irrelevant. The mode selection rule in this case is governed by the boosted bifurcation process (BBP), where the effective bifurcation parameter determining the instability of the fixed point is given as $(|\alpha_1| + \alpha_2)\mu$ instead of $(\alpha_1 + \alpha_2)\mu$. In the range that α_1 is sufficiently smaller than α_{th} but still larger than $-\alpha_2$, the relevant condition is given as t_1/t_2 =odd/even, and t_1/t_2 =odd/odd and even/odd are irrelevant. The mode selection rule in this case obeys the anomalous bifurcation process (ABP), and the first bifurcation occurs in the range $\mu f'(x) > 0$. Thus, the bifurcation is not triggered by the period-doubling bifurcation and is anomalous in this sense.

In the previous work,[20] we gave an intuitive explanation for the bifurcation mechanisms governed by BBP and ABP together with NBP by using linear stability analysis. The purpose of this paper is to give a more rigorous explanation for these bifurcation mechanisms in terms of multidimensional maps embedded in the two-delay system. For each of the relevant and irrelevant conditions $t_1/t_2 = n/m$, the two-delay system is reduced to an individually different m-dimensional map in the nondispersive limit, i.e., a singular perturbation limit (for details, see Sects. 2 and 3). Thus, we investigate the mode selection rules in the NBP, BBP, and ABP regimes in terms of the multidimensional maps. Furthermore, we explore how bifurcation diagrams after the first bifurcation are controlled by the multidimensional maps in the NBP, BBP, and ABP regimes.

This paper is organized as follows.

In Sect. 2, we introduce the two-delay system (1), which has a positive feedback with a long delay time t_2 and either a positive or negative feedback with a short delay time t_1, i.e., $0 < t_1 < t_2$. The strengths of the short and long delays are denoted by α_1 and $\alpha_2(> 0)$, respectively, where we consider the case $-\alpha_2 < \alpha_1 \leq \alpha_2$ when α_2 is fixed. We introduce a control parameter μ and a large constant γ [see Eq. (1)]. To study mode selection rules for the two-delay system, we observe oscillations excited by the first bifurcation as μ is increased adiabatically and we numerically confirm the following. For the system with two positive delays, i.e., $0 < \alpha_1 \leq \alpha_2$, the first bifurcation is governed by NBP. For the system with positive and negative delays, i.e., $-\alpha_2 < \alpha_1 < 0$, the mode selection rule depends on α_1.[20] That is, if α_1 is larger than the threshold α_{th}, it is governed by BBP. If α_1 is sufficiently less than α_{th}, it is governed by ABP.

In Sect. 3, we introduce multidimensional maps of the relevant and irrelevant conditions for the nondispersive system. The nondispersive system is the two-delay system (1) in the limit of $\gamma \to \infty$, i.e., a singular perturbation limit, and is reduced to a two-to-one map (9) if the ratio t_1/t_2 is a rational number, $t_1/t_2 = n/m$, namely, either a relevant or irrelevant condition. Further, the two-to-one map is equivalent to an m-dimensional map. From numerical evidence, we assume that the properties of the two-delay system with a finite γ, i.e., the dispersive system, are well captured by those of the m-dimensional maps. Thus, we focus on three simple cases of $t_1/t_2 = 1/3$, $1/2$, and $2/3$, which exchange the roles of the relevant and irrelevant conditions in the NBP, BBP, and ABP regimes. In terms of the multidimensional maps, the first bifurcation for the relevant condition is regarded as either a pitchfork or period-doubling bifurcation, while a Hopf bifurcation occurs under the irrelevant conditions.

In Sect. 4, we numerically study the bifurcation of the nondispersive system at $t_1/t_2 = 1/3$, $1/2$, and $2/3$. First, we confirm that either a pitchfork or period-doubling bifurcation arises at the first bifurcation for the relevant condition and a Hopf bifurcation is observed for the irrelevant conditions. The first bifurcation for the relevant condition arises at a smaller value in μ than those for the irrelevant conditions. We also study bifurcation diagrams after the first bifurcation with increasing μ. In the range $\alpha_1 > 0$, the first bifurcation is governed by NBP and no important bifurcation occurs after the first bifurcation. At $\alpha_1 = -0.5\alpha_2 > \alpha_{th}$, the first bifurcation is governed by BBP and the motion changes to a chaotic attractor through some bifurcations, but finally changes to locking motion on a torus. At $\alpha_1 = -0.9\alpha_2 < \alpha_{th}$, the first bifurcation governed by ABP occurs in the range $f'(x_c) > 0$ and the motion changes to a chaotic attractor through some bifurcations, but finally changes to locking motion on a torus. After the first bifurcation, the fixed point is restabilized in the range $f'(x_c) > 0$ and a subdominant attractor arises around it, while the dominant attractor created by the first bifurcation exists independently. Furthermore, the fixed point bifurcates again in the range $f'(x_c) < 0$ and the bifurcation is governed by BBP. The subdominant attractors exist only in limited ranges of μ for all three cases, $t_1/t_2 = 1/3$, $1/2$, and $2/3$.

In Sect. 5, we show numerical results for the dispersive system in comparison with those in Sect. 4. First, we explain the relation between the solutions of the nondispersive and dispersive systems. We find the following. The properties of the first bifurcation of the fixed point for the nondispersive system almost hold for the dispersive system. That is, the mode selection rules can be predicted from the analysis of the nondispersive system. Furthermore, as μ increases, the global structure of transitions among attractors is well captured by that of the multidimensional maps. For regular attractors, waveforms are interpreted from solutions of

the multidimensional maps, ignoring some exceptional cases, although irregular oscillations with high-frequency components are observed as the counterparts of chaotic motion for the multidimensional maps. The subdominant attractors in the ABP regime are maintained for the dispersive system, and the existence of the subdominant attractors is not restricted to the three simple cases, $t_1/t_2 = 1/3$, $1/2$, and $2/3$. Namely, it is numerically confirmed for the dispersive system that the subdominant attractors exist in almost all the range of $0 < t_1/t_2 < 1$. Section 6 is devoted to a discussion.

2. Two-Delay System and Mode Selection Rules

2.1 Model system with two delays

The model system, which we treat in this paper, is given by[18)]

$$\frac{1}{\gamma}\frac{dx}{dt} = -x + \mu\alpha_1 f[x(t-t_1)] + \mu\alpha_2 f[x(t-t_2)], \tag{1}$$

where μ is a control parameter and γ is a large constant. The delay time t_2 is fixed as $t_2 = 1$ and t_1 is set as $0 < t_1 < t_2$. The strength α_2 is fixed as $\alpha_2 = 1$ and α_1 is set as $-\alpha_2 < \alpha_1 \leq \alpha_2$. Then, for $\alpha_1 < 0$, the system has positive and negative feedback loops. The function $f(x)$ is given by

$$f(x) = \exp\left[-\frac{(x-x_0)^2}{\Delta x^2}\right]. \tag{2}$$

In the limit of $\gamma \to \infty$, the system is reduced to

$$x(t) = \mu\alpha_1 f[x(t-t_1)] + \mu\alpha_2 f[x(t-t_2)], \tag{3}$$

which is called the nondispersive system, and the system with a finite γ is called the dispersive system.[20)] This limit is a singular perturbation limit of the time-delay system because the differential equation with two delays is reduced to an algebraic equation connecting $x(t-t_1)$ and $x(t-t_2)$ at the two past times to $x(t)$ at the present time. Therefore, we have to carefully handle the relation between the solutions of the dispersive and nondispersive systems, as discussed later.

For the single-delay system with $\alpha_1 = 0$ and $\alpha_2 = 1$, the nondispersive system in Eq. (3) is regarded as a one-dimensional (1D) map,

$$x_i = \mu f(x_{i-1}), \tag{4}$$

and the fixed point x_c is obtained from $x_c = \mu f(x_c)$ at a given value of μ. As shown in Fig. 1, for the case of $x_0 = 0.2$ and $\Delta x = 0.5$, a period-doubling bifurcation occurs only once at $\mu \approx 0.622$, where the condition $\mu f'(x_c) = -1$ is satisfied, and it triggers a Hopf bifurcation

for the single-delay system given by Eq. (1) with $\alpha_1 = 0$, which excites a rounded rectangular wave with period $T \approx 2t_2$. Let us call the map defined by Eq. (4) the embedded map of the single-delay system. Note that μ is a monotonically increasing function of x_c at $x_0 = 0.2$ and $\Delta x = 0.5$.[18)]

As shown in the previous works,[6,9,18,20)] even for the two-delay system, the basic property of the bifurcation of the solution is still governed by the map (4), and the instability of the fixed point of the map triggers a Hopf bifurcation for the solution. The fixed point of the two-delay system is obtained as a solution of the equation

$$x_c = \mu(\alpha_1 + \alpha_2) \exp\left[-\frac{(x_c - x_0)^2}{\Delta x^2}\right], \tag{5}$$

and $f'(x_c)$ is given by

$$f'(x_c) = -\frac{2(x_c - x_0)}{\Delta x^2} \exp\left[-\frac{(x_c - x_0)^2}{\Delta x^2}\right] = -\frac{2(x_c - x_0)x_c}{\mu(\alpha_1 + \alpha_2)\Delta x^2}. \tag{6}$$

We introduce a variable $\bar{\eta}$ defined as

$$\bar{\eta} \equiv \mu f'(x_c), \tag{7}$$

which plays an important role in considering the difference between the 'relevant' and 'irrelevant' conditions as discussed in the following sections.

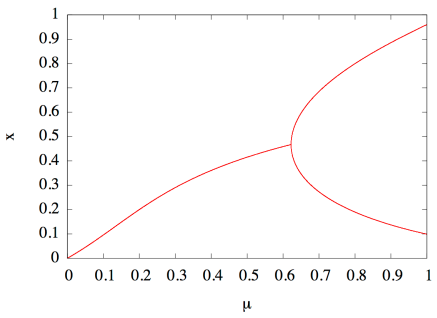

Fig. 1. (Color online) Bifurcation diagram of the 1D map (4) with $x_0 = 0.2$ and $\Delta x = 0.5$. A period-doubling bifurcation occurs at $\mu \approx 0.622$.

2.2 Mode selection rule

As shown by the previous works,[6,9,18,20)] the oscillation mode excited by the first bifurcation changes with the ratio t_1/t_2, and a clear mode selection rule as a function of t_1/t_2 exists if α_1 is fixed, but it changes with α_1. To understand the mode selection rule, the notion of relevant and irrelevant conditions is important. The relevant and irrelevant conditions are rational numbers $t_1/t_2 = n/m$ for the nondispersive system. For the dispersive system, they slightly

shift as

$$t_1 = \frac{n}{m} t_2 \quad \rightarrow \quad t_1' = \frac{n}{m} t_2 + \Delta t_\gamma, \tag{8}$$

where $\Delta t_\gamma \approx -\gamma^{-1}(1 - t_1/t_2) = -\gamma^{-1}(1 - n/m)$.[19)]

For the nondispersive system, if $t_1/t_2 = n/m$ is the relevant condition, an oscillation with $\omega = m\omega_f$ can be excited by the first bifurcation, where $\omega_f = \pi/t_2$, which is the angular frequency of the fundamental oscillation for the single-delay system. Precisely speaking, the oscillation has frequency components $\omega = (2l + 1)m\omega_f$ ($l = 0, 1, 2, 3, \cdots$) because it is a rectangular wave as discussed in Sect. 3.1. For the dispersive system, oscillations with $\omega \approx m\omega_f$ are observed in a neighborhood of $t_1' = nt_2/m + \Delta t_\gamma$ if $m\omega_f$ is less than the cutoff frequency ω_{cut}, which is roughly estimated as $\omega_{cut} \propto \gamma$.[9,19)]

• Mode selection rule governed by NBP.

For the system with two positive feedback loops, i.e., $0 < \alpha_1 \leq \alpha_2$, the relevant condition is given as t_1/t_2 =odd/odd, and the irrelevant conditions are given by t_1/t_2 =even/odd and odd/even.[6,9,18,20)] Let us see the numerical results for the dispersive system with $\gamma = 210$. To detect the first bifurcation mode numerically, the control parameter μ is increased almost adiabatically with the rate $d\mu/dt = 4.2 \times 10^{-5}$. Figure 2(a) shows the normalized frequency ω/ω_f of the first excited mode as a function of t_1/t_2. In a neighborhood of a relevant condition $t_1/t_2 = (2n + 1)/(2m + 1)$, e.g., $t_1/t_2 = 1/3$, $1/5$, and $3/5$, oscillations with $\omega \approx (2m+1)\omega_f$, i.e., $(2m+1)$-th harmonic, are excited when α_1 is sufficiently large. In a neighborhood of an irrelevant condition $t_1/t_2 = (2n + 1)/(2m)$ or $(2n)/(2m + 1)$, e.g., $t_1/t_2 = 1/2$ and $2/3$, twin peaks consisting of higher-order odd harmonics, called the tower structure, exist, which is the noteworthy characteristic induced by the irrelevant condition, although a lower harmonic wave is observed at the center of the tower structure, i.e., the irrelevant condition for the dispersive system given by Eq. (8). As α_1 becomes smaller, lower-order modes dominate, and at $\alpha_1 = 0.001$, the fundamental mode appears in almost all the range $0 < t_1/t_2 < 0$ because the system is close to the single-delay system. The bifurcation process controlling the mode selection rule of the system with two positive feedback loops is called NBP.[20)] For a relevant condition with $(2m + 1)\omega_f < \omega_{cut}$, the first bifurcation is induced by the period-doubling bifurcation of the 1D map (4) with μ replaced by $\mu(\alpha_1 + \alpha_2)$, and the bifurcation point μ_{NR} is approximately obtained from the condition $\mu(\alpha_1 + \alpha_2)f'(x_c) = -1$.[20)] The bifurcation points μ_{NI} for irrelevant conditions are normally larger than μ_{NR}.

• Mode selection rule governed by BBP.

For the system with positive and negative delay feedback loops, i.e., $-\alpha_2 < \alpha_1 < 0$, two bi-

furcation processes different from NBP exist, i.e., BBP and ABP, which control the mode selection rule in turn with decreasing α_1.[20] BBP dominates when α_1 is larger than the threshold $\alpha_{th} \approx -0.851\alpha_2$. In the BBP regime $(\alpha_{th} < \alpha_1 < 0)$, the relevant condition is t_1/t_2 =even/odd, and the irrelevant conditions are given by t_1/t_2 =odd/odd and odd/even. As shown in Fig. 2(b), the distribution of the normalized frequencies is an almost horizontal inversion of that of NBP. For the relevant condition of BBP, the bifurcation point μ_{BR} is approximately given by the condition $\mu(|\alpha_1| + \alpha_2)f'(x_c) = -1$, but the fixed point x_c is given by Eq. (5).[20]

• Mode selection rule governed by ABP.

In the range $-\alpha_2 < \alpha_1 \leq -0.9\alpha_2 < \alpha_{th}$, the mode selection rule obeys ABP. In the ABP regime, the relevant condition is t_1/t_2 =odd/even, and the irrelevant conditions are given by t_1/t_2 =odd/odd and even/odd. As shown in Fig. 2(c), the distribution of the normalized frequencies is almost bilaterally symmetric and is completely different from that of BBP. For the relevant condition of ABP, the bifurcation point μ_{AR} is approximately given by the condition $\mu(|\alpha_1| + \alpha_2)f'(x_c) = +1$, which cannot be explained by the period-doubling bifurcation of the map (4). In the previous work,[20] we explained the mechanisms of BBP and ABP by linear stability analysis. In the following sections, we give a clearer explanation of the mechanisms of BBP and ABP by using multidimensional maps embedded in a nondispersive system.

• Mixed regime of BBP and ABP.

Note that in the range $-0.9\alpha_2 < \alpha_1 < \alpha_{th}$, the mode selection rule depends on the rate t_1/t_2. In a neighborhood of a relevant condition of ABP, $t_1/t_2 = (2n + 1)/2m$ with a small natural number m, ABP takes the place of BBP at an early stage as α_1 decreases, but in a neighborhood of an irrelevant condition of ABP, $t_1/t_2 = 2n/(2m + 1)$ or $(2n + 1)/(2m + 1)$ with a small nonnegative integer m, BBP changes to ABP at a later stage.

3. Multidimensional Maps of the Relevant and Irrelevant Conditions for the Nondispersive System

3.1 Solutions for the relevant and irrelevant conditions in the nondispersive limit

At each of the relevant and irrelevant conditions for the nondispersive system, t_1/t_2 is a rational number, $t_1/t_2 = n/m$, where n/m is an irreducible fraction. Then, we introduce a discrete-time system with an interval $\Delta t = t_2/m$ and define x_j as $x_j = x(j\Delta t + t_0)$, where the initial time t_0 is chosen arbitrarily. Equation (3) is reduced to the following two-to-one map,

$$x_j = \mu[\alpha_1 f(x_{j-n}) + \alpha_2 f(x_{j-m})]. \tag{9}$$

(a)

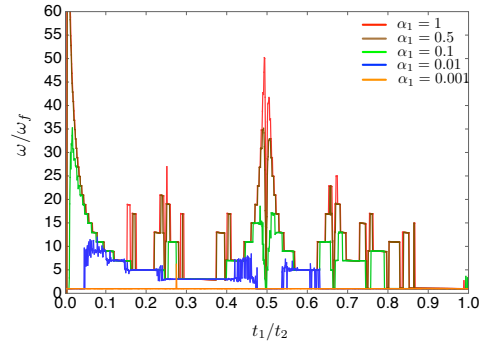

(b)

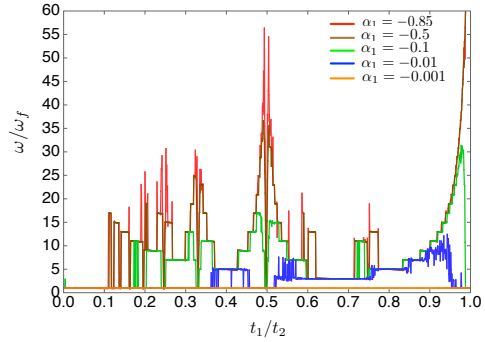

(c)

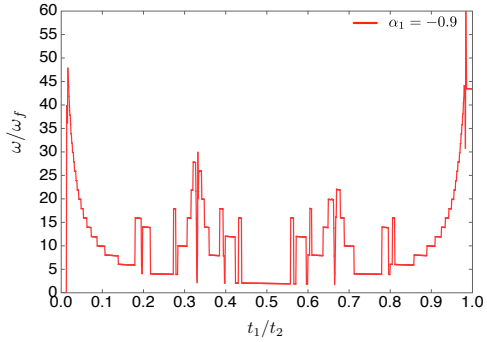

Fig. 2. (Color online) Normalized frequency ω/ω_f of the first excited mode as a function of t_1/t_2 at $\gamma = 210$ and $\alpha_2 = 1$ when μ is increased with the rate $d\mu/dt = 4.2 \times 10^{-5}$. (a) Normal bifurcation process (NBP). (b) Boosted bifurcation process (BBP). (c) Anomalous bifurcation process (ABP).

If an initial sequence $\{x_0, x_1, \cdots, x_{m-1}\}$ is given, the map (9) generates a semi-infinite sequence $\{x_0, x_1, \cdots, x_j, x_{j+1}, \cdots\}$.

For the single-delay system with $\alpha_1 = 0$ and $t_1/t_2 = 1$, the two-to-one map (9) is reduced to the 1D map (4). The period-doubling bifurcation creates a period-2 cycle, $\{x_-, x_+, x_-, x_+, \cdots\}$, and the solution is periodic with period $2t_2$ for the time-continuous system (3). The simplest solution is a rectangular wave with period $2t_2$ as shown in Fig. 3(a). This is the fundamental

wave with fundamental period $T_f = 2\pi/\omega_f = 2t_2$. Note that in the interval $t_0 \le t < t_0 + t_2$ for a given t_0, the solution can arbitrarily take either x_+ or x_- point by point. For example, a solution may take x_+ on the rational points and x_- on the irrational points, and it may take the opposite choice for the next interval. However, such a solution is unphysical for the dispersive system. Thus, the rectangular wave is a reasonable solution corresponding to the solution of the dispersive system, which is a rounded rectangular wave with period $T \approx T_f$.[20)]

Let us consider the case that $|\alpha_1|$ is nonzero and sufficiently large. For the two-delay system in the nondispersive limit, a rectangular wave with the unit step width t_2/m should be observed at the relevant condition $t_{1R}/t_2 = n/m$ and is regarded as an mth-order mode.[20)] For example, Fig. 3(b) shows the 3rd-order mode at $t_{1R}/t_2 = 1/3$ in the NBP regime: owing to the period doubling bifurcation of the two-to-one map (9), $x(t - t_2) = x_{i-3} = x_+$ and $x(t - t_1) = x_{i-1} = x_+$ are mapped to $x(t) = x_i = x_-$. For the dispersive system, if m is sufficiently small compared with γ, there exists a neighborhood of the relevant condition, in which rounded rectangular waves each with period $T \approx T_f/m$ are excited as shown in Fig. 4.[6,9,18,20)]

For the nondispersive system, the first bifurcation point at the irrelevant condition μ_I is larger than that at the relevant condition μ_R if $|\mu f'(x_c)|$ is a monotonically increasing function of μ in a neighborhood of the first bifurcation point.[20)] It means that for the nondispersive system, $|\bar{\eta}_\infty| = |\mu f'(x_c)|$ in Eq. (7) at the first bifurcation for the irrelevant condition $t_{1I}/t_2 = n'/m'$ is larger than that for the relevant condition $t_{1R}/t_2 = n/m$, although it changes with t_{1I}/t_2.[18,20)] Note that $\bar{\eta}_\infty$ at the first bifurcation for the relevant conditions for NBP, BBP, and ABP are given as $\bar{\eta}_\infty = -1/(\alpha_1 + \alpha_2)$, $-1/(|\alpha_1| + \alpha_2)$, and $1/(|\alpha_1| + \alpha_2)$, respectively (see Sec. 2.2). For the dispersive system, at the irrelevant condition defined by Eq. (8), i.e., $t_1 = t_{1I} + \Delta t_\gamma$, if m' is sufficiently small to generate the tower structure around it, $|\bar{\eta}_\gamma| = |\mu f'(x_c)|$ in Eq. (7) at the first bifurcation takes the local maximum value such that $|\bar{\eta}_\gamma(t_{1I} + \Delta t_\gamma)| = |\bar{\eta}_\infty(t_{1I})| + |O(m'^2/\gamma^2)|$.[18,20)] Note that at the relevant condition for the dispersive system if m is sufficiently small, $|\bar{\eta}_\gamma|$ takes the local minimum value such that $|\bar{\eta}_\gamma(t_{1R} + \Delta t_\gamma)| = |\bar{\eta}_\infty(t_{1R})| + |O(m^2/\gamma^2)|$.[18,20)]

From the above discussion, we give the following assumptions (also see Fig. 4).

A1: Assume that $t_{1R}/t_2 = n/m$ is a relevant condition for the nondispersive system. For the dispersive system with a given γ, if there exists a neighborhood of the relevant condition $t_1 = t_{1R} + \Delta t_\gamma$ in which oscillations excited by the first bifurcation are rounded rectangular waves each with period $T \approx T_f/m$, then, in the limit $\gamma \to \infty$, the neighborhood converges

to t_{1R} and the rounded rectangular waves converge to the rectangular wave with period $T = T_f/m$.

A2: Assume that $t_{1I}/t_2 = n'/m'$ is an irrelevant condition for the nondispersive system. For the dispersive system with a given γ, if the tower structure exists in a neighborhood of the irrelevant condition $t_1 = t_{1I} + \Delta t_\gamma$, then, in the limit $\gamma \to \infty$, $\bar{\eta}_\gamma$ converges to $\bar{\eta}_\infty$ along the path $t_1 = t_{1I} + \Delta t_\gamma \to t_1 = t_{1I}$.

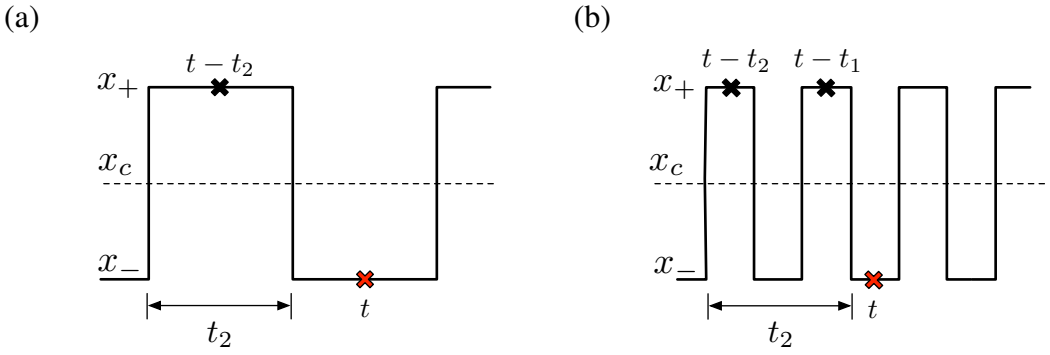

Fig. 3. (Color online) Waves observed for the nondispersive system. (a) Wave for the single-delay system. (b) Wave induced by NBP at $t_1/t_2 = 1/3$.

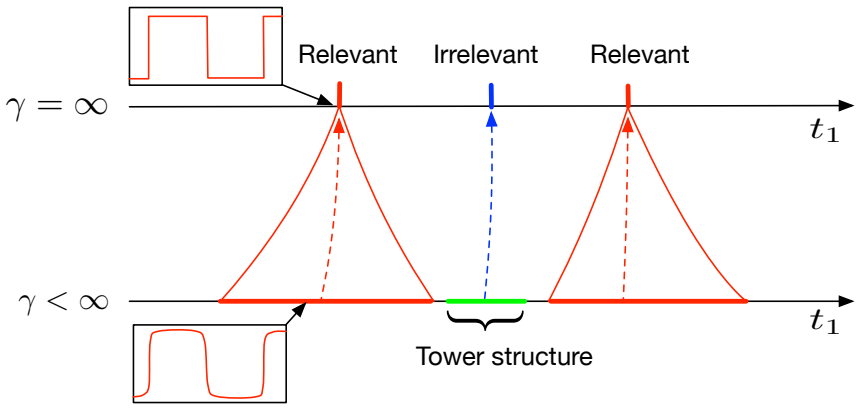

Fig. 4. (Color online) Correspondence between solutions of the dispersive and nondispersive systems.

3.2 Theoretical analyses of multidimensional maps on the relevant and irrelevant conditions

At $t_1/t_2 = n/m$, where n/m is an irreducible fraction, i.e., either a relevant or irrelevant condition for the nondispersive system, we need an m-dimensional space to transform the two-to-one map (9) to a one-to-one map. For a sequence $(x_0, x_1, \cdots, x_n, x_{n+1}, \cdots)$ created by

the two-to-one map (9), the first m elements $\boldsymbol{X}_0 = (x_0, x_1, \cdots, x_{m-1})$ are regarded as an initial vector in the m-dimensional space and the next interval $\boldsymbol{X}_1 = (x_m, x_{m+1}, \cdots, x_{2m-1})$ is obtained from $\boldsymbol{X}_0$. Therefore, the vector of the i-th interval $\boldsymbol{X}_i$ defined by

$$\boldsymbol{X}_i = (x_{mi}, x_{mi+1}, \cdots, x_{mi+m-1}) \tag{10}$$

is obtained from the vector of the (i-1)-th interval $\boldsymbol{X}_{i-1}$ by an m-dimensional map $\boldsymbol{F}$ as

$$\boldsymbol{X}_i = \boldsymbol{F}(\boldsymbol{X}_{i-1}). \tag{11}$$

Then, a single iteration of the m-dimensional map $\boldsymbol{F}$ corresponds to the time interval t_2.

At every rational number in t_1/t_2, a different one-to-one map exists. Thus, it is practically impossible to handle all the one-to-one maps. In this paper, we focus on three simple cases, $t_1/t_2 = 1/2$, $1/3$, and $2/3$, which exchange the roles of the relevant and irrelevant conditions for NBP, BBP, and ABP as shown in Table I.

Table I. Relevant and irrelevant conditions for the three bifurcation processes.

t_1/t_2	NBP	BBP	ABP
1/3	Relevant	Irrelevant	Irrelevant
1/2	Irrelevant	Irrelevant	Relevant
2/3	Irrelevant	Relevant	Irrelevant

3.2.1 Map for the condition $t_1/t_2 = 1/2$

In the case of $t_1/t_2 = 1/2$, the map (9) is represented as

$$x_{j+1} = \mu\alpha_1 f(x_j) + \mu\alpha_2 f(x_{j-1}). \tag{12}$$

By introducing new variables $y_i = x_{2i}$ and $z_i = x_{2i+1}$, the two-to-one map (12) is transformed to a two-dimensional (2D) map:

$$\begin{aligned} y_{i+1} &= \mu\alpha_1 f(z_i) + \mu\alpha_2 f(y_i), \\ z_{i+1} &= \mu\alpha_1 f(y_{i+1}) + \mu\alpha_2 f(z_i) \\ &= \mu\alpha_1 f(\mu\alpha_1 f(z_i) + \mu\alpha_2 f(y_i)) + \mu\alpha_2 f(z_i). \end{aligned} \tag{13}$$

The fixed point (y_c, z_c) of the 2D map (13) satisfies the following equations:

$$\begin{aligned} y_c &= \mu\alpha_1 f(z_c) + \mu\alpha_2 f(y_c), \\ z_c &= \mu\alpha_1 f(y_c) + \mu\alpha_2 f(z_c). \end{aligned} \tag{14}$$

The fixed point x_c of the two-to-one map (12) given by $x_c = \mu(\alpha_1+\alpha_2)f(x_c)$ corresponds to the fixed point with $y_c = z_c = x_c$ of the 2D map (13) satisfying Eq. (14). In particular, if $\alpha_1 = \alpha_2$, Eq. (14) indicates that (x_c, x_c) is the only fixed point. If $y_c \neq z_c$ for $0 < |\alpha_1| < \alpha_2$, there is a pair of fixed points (y_c, z_c) and (z_c, y_c) due to the symmetry, each of which corresponds to a period-2 cycle of the map (12), namely, $x_{2i} = y_c$ (z_c), $x_{2i+1} = z_c$ (y_c). To investigate the bifurcation of the fixed point of the map (12), we have to analyze the bifurcation of the fixed point (x_c, x_c) of the 2D map (13).

To consider the stability of the fixed point (x_c, x_c), we examine the behavior of a point close to the fixed point, i.e., $y_i = x_c + \delta y_i$, $z_i = x_c + \delta z_i$, by using linear stability analysis. The variational equation around the fixed point is given by

$$\begin{aligned}
\delta y_{i+1} &= \mu f'(x_c)(\alpha_1 \delta z_i + \alpha_2 \delta y_i), \\
\delta z_{i+1} &= \mu f'(x_c)(\alpha_1 \delta y_{i+1} + \alpha_2 \delta z_i) \\
&= \mu f'(x_c)(\mu f'(x_c)\alpha_1\alpha_2 \delta y_i + (\mu f'(x_c)\alpha_1^2 + \alpha_2)\delta z_i).
\end{aligned} \tag{15}$$

Then, we need to obtain the eigenvalues λ of the matrix

$$A = \mu f'(x_c) \begin{pmatrix} \alpha_2 & \alpha_1 \\ \mu f'(x_c)\alpha_1\alpha_2 & \mu f'(x_c)\alpha_1^2 + \alpha_2 \end{pmatrix}, \tag{16}$$

and bifurcation points are obtained from the condition $|\lambda| = 1$. Let us define λ' as $\lambda = \mu f'(x_c)\lambda'$. Thus, our task is to obtain λ' satisfying the following characteristic polynomial,

$$\begin{vmatrix} \alpha_2 - \lambda' & \alpha_1 \\ \mu f'(x_c)\alpha_1\alpha_2 & \mu f'(x_c)\alpha_1^2 + \alpha_2 - \lambda' \end{vmatrix} = 0, \tag{17}$$

which is rewritten as

$$\lambda'^2 - (\mu f'(x_c)\alpha_1^2 + 2\alpha_2)\lambda' + \alpha_2^2 = 0. \tag{18}$$

The solutions of Eq. (18) are given as

$$\lambda' = \frac{1}{2}\Big[\mu f'(x_c)\alpha_1^2 + 2\alpha_2 \pm \sqrt{(\mu f'(x_c)\alpha_1^2 + 2\alpha_2)^2 - 4\alpha_2^2}\Big]. \tag{19}$$

Since the solution for the map (12) at a relevant condition becomes a period-2 cycle after the bifurcation, the bifurcation of the 2D map should be either a pitchfork or period-doubling bifurcation, namely, $\lambda = \pm 1$ and $\lambda' \in \mathbb{R}$. Thus, the discriminant of Eq. (18) takes a positive value:

$$\mu^2 f'(x_c)^2 \alpha_1^4 + 4\alpha_2\alpha_1^2 \mu f'(x_c) > 0, \tag{20}$$

which is always satisfied for $f'(x_c) > 0$, but is reduced to $\mu f'(x_c) < -4\alpha_2/\alpha_1^2$ for $f'(x_c) < 0$,

namely, $|\mu f'(x_c)| > 4\alpha_2/\alpha_1^2$.

For $f'(x_c) > 0$, Eq. (19) gives $\lambda' > 0$ and $\lambda > 0$. Thus, if bifurcation occurs, it is a pitchfork bifurcation with $\lambda = 1$ and the period-doubling bifurcation with $\lambda = -1$ is prohibited. Using the variable $\bar{\eta}$ defined by Eq. (7), Eq. (19) at the bifurcation point with $\lambda = 1$ is rewritten as

$$\begin{aligned} \frac{2}{\bar{\eta}} &= \bar{\eta}\alpha_1^2 + 2\alpha_2 \pm \sqrt{(\bar{\eta}\alpha_1^2 + \alpha_2)^2 - 4\alpha_2^2} \\ &\Rightarrow (\alpha_2^2 - \alpha_1^2)\bar{\eta}^2 - 2\alpha_2\bar{\eta} + 1 = 0, \end{aligned} \tag{21}$$

and the root $\bar{\eta}$ is given by

$$\bar{\eta} = \mu f'(x_c) = \frac{1}{\alpha_2 \mp \alpha_1}. \tag{22}$$

For $\alpha_1 < 0$, the root (22) with a minus sign is smaller than that with a plus sign and the former bifurcation occurs earlier than the latter if $f'(x_c(\mu))$ is a monotonically increasing function of μ. Since x_c is a function of μ, the values of μ and x_c at the bifurcation point are obtained from the condition

$$\mu(\alpha_2 - \alpha_1)f'(x_c) = \mu(\alpha_2 + |\alpha_1|)f'(x_c) = 1, \tag{23}$$

which is simply the condition of the first bifurcation for the relevant condition in the ABP regime.[20] For the case of $0 < \alpha_1 \leq \alpha_2$, the bifurcation given by Eq. (22) with a plus sign arises earlier than the other if $f'(x_c(\mu))$ is a monotonically increasing function of μ.

For $\mu f'(x_c) < -4\alpha_2/\alpha_1^2$, λ' given by Eq. (19) always takes negative values and $\lambda(= \mu f'(x_c)\lambda')$ becomes positive. Thus, the period-doubling bifurcation with $\lambda = -1$ is prohibited. The same discussion as that for $f'(x_c) > 0$ is applied for this case and the bifurcation point with $\lambda = 1$ should be given by Eq. (22), which indicates that $\mu f'(x_c)$ takes a positive or infinite value for $|\alpha_1| \leq \alpha_2$ and contradicts the assumption $f'(x_c) < 0$. Hence, the pitchfork bifurcation with $\lambda = 1$ does not occur for $f'(x_c) < 0$.

To consider the other eigenvalue at the bifurcation point with $\lambda = 1$, we substitute Eq. (22) into Eq. (19). For $\mu f'(x_c) = 1/(\alpha_2 - \alpha_1)$, we obtain the following eigenvalues:

$$\begin{aligned} \lambda'_{1-} &= \alpha_2 - \alpha_1, \quad \rightarrow \quad \lambda_{1-} = \mu f'(x_c)\lambda'_{1-} = 1, \\ \lambda'_{2-} &= \frac{\alpha_2^2}{\alpha_2 - \alpha_1}, \quad \rightarrow \quad \lambda_{2-} = \mu f'(x_c)\lambda'_{2-} = \frac{\alpha_2^2}{(\alpha_2 - \alpha_1)^2}. \end{aligned} \tag{24}$$

The latter is the eigenvalue under consideration. Since $\lambda_{2-} < \lambda_{1-}$ for $\alpha_1 < 0$, the fixed point is stable before the pitchfork bifurcation and it becomes a hyperbolic fixed point after the bifurcation. Since $\lambda_{2-} > \lambda_{1-}$ for $\alpha_2 > \alpha_1 > 0$, the fixed point is already hyperbolic before the bifurcation and changes to an unstable fixed point after it. For $\mu f'(x_c) = 1/(\alpha_2 + \alpha_1)$, the

eigenvalues are obtained as

$$\begin{aligned} \lambda'_{1+} &= \alpha_2 + \alpha_1, \quad \rightarrow \quad \lambda_{1+} = \mu f'(x_c)\lambda'_{1+} = 1, \\ \lambda'_{2+} &= \frac{\alpha_2^2}{\alpha_2 + \alpha_1}, \quad \rightarrow \quad \lambda_{2+} = \mu f'(x_c)\lambda'_{2+} = \frac{\alpha_2^2}{(\alpha_2 + \alpha_1)^2}. \end{aligned} \tag{25}$$

Since $\lambda_{2+} < \lambda_{1+}$ for $\alpha_1 > 0$, the fixed point is stable before the bifurcation and hyperbolic after it. For $-\alpha_2 < \alpha_1 < 0$, it changes from a hyperbolic fixed point to a unstable fixed point through the bifurcation because $\lambda_{2+} > \lambda_{1+}$. If $f'(x_c(\mu))$ is a monotonically increasing function of μ, a bifurcation with λ_{1-} (λ_{1+}) is the first bifurcation for $\alpha_1 < 0$ ($\alpha_1 > 0$).

Finally, we discuss the condition that the Hopf bifurcation occurs. In this case, the eigenvalues λ and λ^* are nonreal complex conjugates and satisfy the condition $\lambda\lambda^* = 1$. Thus, the discriminant (20) takes a negative value and $f'(x_c) < 0$. From Eq. (19), the condition $\lambda\lambda^* = 1$ is written as

$$\lambda\lambda^* = \mu^2 f'(x_c)^2 \alpha_2^2 = 1, \tag{26}$$

and, taking $f'(x_c) < 0$ into account, we obtain

$$\mu f'(x_c)\alpha_2 = -1, \tag{27}$$

which gives the bifurcation point at the irrelevant condition $t_1/t_2 = 1/2$ for the nondispersive system and is the same as that obtained with the linear mode stability analysis for Eq. (1) in the limit $\gamma \to \infty$, which was studied in our previous work.[20] Note that the condition (27) is independent of α_1. From Eqs.(19) and (27), λ at the Hopf bifurcation is obtained as

$$\begin{aligned} \lambda &= \mu f'(x_c)\lambda' \\ &= \frac{1}{2}\Big[\alpha_1^2/\alpha_2^2 - 2 \mp \sqrt{(\alpha_1^2/\alpha_2^2 - 2)^2 - 4}\Big]. \end{aligned} \tag{28}$$

At $\alpha_1/\alpha_2 = 1$, it is reduced to

$$\lambda = -\frac{1}{2}\Big(1 \pm \sqrt{-3}\Big), \tag{29}$$

which gives a period-3 cycle because $\lambda^3 = 1$.

3.2.2 2D map of $t_1/t_2 = 1/2$ including the function (2)

From the discussion in Sect. 3.2.1, the period-doubling bifurcation with $\lambda_1 = -1$ is prohibited and the pitchfork bifurcation with $\lambda_1 = 1$ is possible only for $f'(x_c) > 0$. Let us consider the condition of the pitchfork bifurcation for the 2D map including the function (2). Combining Eq. (22) with Eq. (6) gives a quadratic equation of x_c,

$$\frac{2(x_c - x_0)x_c}{(\alpha_1 + \alpha_2)\Delta x^2} = -\frac{1}{\alpha_2 \pm \alpha_1}. \tag{30}$$

If a plus sign is taken, Eq. (30) is reduced to

$$2x_c^2 - 2x_0x_c + \Delta x^2 = 0, \tag{31}$$

and the discriminant $d = x_0^2 - 2\Delta x^2$ takes a negative value for $x_0 = 0.2$, $\Delta x = 0.5$; thus, x_c is not a real solution and the bifurcation with $\lambda_1 = 1$ is prohibited. When a minus sign is chosen, Eq. (30) is reduced to

$$2x_c^2 - 2x_0x_c + \frac{\alpha_2 + \alpha_1}{\alpha_2 - \alpha_1}\Delta x^2 = 0, \tag{32}$$

and x_c at the bifurcation is given by

$$x_c = \frac{1}{2}\left(x_0 \pm \sqrt{x_0^2 - 2\bar{\alpha}\Delta x^2}\right), \tag{33}$$

where $\bar{\alpha} \equiv \frac{\alpha_2+\alpha_1}{\alpha_2-\alpha_1}$. To obtain a real-valued x_c, the discriminant must be real and we obtain

$$\frac{x_0^2}{2\Delta x^2} \geq \bar{\alpha} = \frac{\alpha_2 + \alpha_1}{\alpha_2 - \alpha_1}, \tag{34}$$

which is reduced to

$$\alpha_1 \leq \frac{\bar{\alpha}_c - 1}{\bar{\alpha}_c + 1}\alpha_2 \equiv \alpha_{th}, \tag{35}$$

where $\bar{\alpha}_c \equiv \frac{x_0^2}{2\Delta x^2}$ and α_{th} is the threshold value. This is simply the condition of the first bifurcation in the ABP regime.[20] For $x_0 = 0.2$ and $\Delta x = 0.5$, the right-hand side of Eq. (35) takes a negative value because $\bar{\alpha}_c < 1$. Then, the pitchfork bifurcation does not occur for $\alpha_1 > \alpha_{th}(< 0)$. From the discussion in Sect. 3.2.1, the absolute value of the other eigenvalue $|\lambda_2|$ is less than one and the pitchfork bifurcation is the first bifurcation for $\alpha_1 < \alpha_{th}$.

For $\alpha_1 > \alpha_{th}$, only the Hopf bifurcation occurs in the range $f'(x_c) < 0$ and the bifurcation point is given by Eq. (27). Combining Eq. (27) with Eq. (6), we obtain

$$\frac{2(x_c - x_0)x_c}{(\alpha_1 + \alpha_2)\Delta x^2} = \frac{1}{\alpha_2}, \tag{36}$$

which is reduced to

$$2x_c^2 - 2x_0x_c - \frac{\alpha_2 + \alpha_1}{\alpha_2}\Delta x^2 = 0. \tag{37}$$

The root x_c is given by

$$x_c = \frac{1}{2}\left(x_0 \pm \sqrt{x_0^2 + 2\frac{\alpha_2 + \alpha_1}{\alpha_2}\Delta x^2}\right). \tag{38}$$

Since $x_c > x_0$ for $f'(x_c) < 0$, a plus sign is selected. As shown later, even in the range $-\alpha_2 < \alpha_1 < \alpha_{th}$, a Hopf bifurcation always occurs at a large value of μ.

3.2.3 *Map for the condition $t_1/t_2 = 1/3$*

In the case of $t_1/t_2 = 1/3$, the map (3) is represented as

$$x_{j+1} = \mu\alpha_1 f(x_j) + \mu\alpha_2 f(x_{j-2}). \tag{39}$$

By introducing the variables $\xi_i = x_{3i}$, $\eta_i = x_{3i+1}$, and $\zeta_i = x_{3i+2}$, Eq. (39) is transformed to a three-dimensional (3D) map:

$$\begin{aligned}
\xi_{i+1} &= \mu\alpha_1 f(\zeta_i) + \mu\alpha_2 f(\xi_i), \\
\eta_{i+1} &= \mu\alpha_1 f(\xi_{i+1}) + \mu\alpha_2 f(\eta_i) \\
&= \mu\alpha_1 f(\mu\alpha_1 f(\zeta_i) + \mu\alpha_2 f(\xi_i)) + \mu\alpha_2 f(\eta_i), \\
\zeta_{i+1} &= \mu\alpha_1 f(\eta_{i+1}) + \mu\alpha_2 f(\zeta_i) \\
&= \mu\alpha_1 f(\mu\alpha_1 f(\mu\alpha_1 f(\zeta_i) + \mu\alpha_2 f(\xi_i)) + \mu\alpha_2 f(\eta_i)) + \mu\alpha_2 f(\zeta_i).
\end{aligned} \tag{40}$$

The fixed point (ξ_c, η_c, ζ_c) of the 3D map (40) satisfies the following equations:

$$\begin{aligned}
\xi_c &= \mu\alpha_1 f(\zeta_c) + \mu\alpha_2 f(\xi_c), \\
\eta_c &= \mu\alpha_1 f(\xi_c) + \mu\alpha_2 f(\eta_c), \\
\zeta_c &= \mu\alpha_1 f(\eta_c) + \mu\alpha_2 f(\zeta_c).
\end{aligned} \tag{41}$$

The fixed point x_c of the two-to-one map (39) becomes the fixed point of the 3D map (40) with $\xi_c = \eta_c = \zeta_c = x_c$. In the case that ξ_c, η_c, and ζ_c are different from each other, there are three fixed points, i.e., (ξ_c, η_c, ζ_c), (η_c, ζ_c, ξ_c), and (ζ_c, ξ_c, η_c), each of which forms a period-3 cycle in the two-to-one map (39). It is easily shown that if any two of ξ_c, η_c, and ζ_c are the same, the remaining one takes the same value, namely, $\xi_c = \eta_c = \zeta_c = x_c$.

The stability of the fixed point (x_c, x_c, x_c) can be determined by linear stability analysis. The variational equation around the fixed point is given as

$$\begin{aligned}
\delta\xi_{i+1} &= \mu f'(x_c)(\alpha_1\delta\zeta_i + \alpha_2\delta\xi_i), \\
\delta\eta_{i+1} &= \mu f'(x_c)(\alpha_1\delta\xi_{i+1} + \alpha_2\delta\eta_i) \\
&= \mu f'(x_c)[\mu f'(x_c)\alpha_1^2\delta\zeta_i + \mu f'(x_c)\alpha_1\alpha_2\delta\xi_i + \alpha_2\delta\eta_i], \\
\delta\zeta_{i+1} &= \mu f'(x_c)(\alpha_1\delta\eta_{i+1} + \alpha_2\delta\zeta_i) \\
&= \mu f'(x_c)[\mu^2 f'(x_c)^2\alpha_1^2\alpha_2\delta\xi_i + \mu f'(x_c)\alpha_1\alpha_2\delta\eta_i + \mu^2 f'(x_c)^2\alpha_1^3\delta\zeta_i + \alpha_2\delta\zeta_i].
\end{aligned} \tag{42}$$

Thus, we need to obtain the eigenvalues λ of the matrix

$$B = \mu f'(x_c) \begin{pmatrix} \alpha_2 & 0 & \alpha_1 \\ \mu f'(x_c)\alpha_1\alpha_2 & \alpha_2 & \mu f'(x_c)\alpha_1^2 \\ \mu^2 f'(x_c)^2\alpha_1^2\alpha_2 & \mu f'(x_c)\alpha_1\alpha_2 & \alpha_2 + \mu^2 f'(x_c)^2\alpha_1^3 \end{pmatrix}. \tag{43}$$

We introduce λ' defined as $\lambda = \mu f'(x_c)\lambda'$, and λ' is a root of the following characteristic polynomial,

$$\begin{vmatrix} \alpha_2 - \lambda' & 0 & \alpha_1 \\ \mu f'(x_c)\alpha_1\alpha_2 & \alpha_2 - \lambda' & \mu f'(x_c)\alpha_1^2 \\ \mu^2 f'(x_c)^2\alpha_1^2\alpha_2 & \mu f'(x_c)\alpha_1\alpha_2 & \alpha_2 + \mu^2 f'(x_c)^2\alpha_1^3 - \lambda' \end{vmatrix} = 0, \tag{44}$$

which is reduced to

$$\begin{aligned} &(\alpha_2 - \lambda')^3 + \mu^2 f'(x_c)^2\alpha_1^3(\alpha_2 - \lambda')^2 + \mu^2 f'(x_c)^2\alpha_1^3\alpha_2^2 - 2\mu^2 f'(x_c)^2\alpha_1^3\alpha_2(\alpha_2 - \lambda') \\ &= (\alpha_2 - \lambda')^3 + \mu^2 f'(x_c)^2\alpha_1^3\lambda'^2 = 0. \end{aligned} \tag{45}$$

First, we consider bifurcations with $\lambda = \pm 1$. Substituting $\mu f'(x_c) = \pm 1/\lambda'$ into Eq. (45), we obtain

$$\begin{aligned} &(\alpha_2 - \lambda')^3 + \alpha_1^3(\alpha_2 - \lambda')^2/\lambda'^2 + \alpha_1^3\alpha_2^2/\lambda'^2 - 2\alpha_1^3\alpha_2(\alpha_2 - \lambda')/\lambda'^2 \\ &= -\lambda'^3 + 3\lambda'^2\alpha_2 - 3\lambda'\alpha_2^2 + \alpha_1^3 + \alpha_2^3 = 0, \end{aligned} \tag{46}$$

and $\lambda'_1 = \alpha_2 + \alpha_1 > 0$ is a root, which is immediately confirmed by substituting it into Eq. (46). The two remaining roots of Eq. (46) are $\lambda'_{2,3} = (2\alpha_2 - \alpha_1 \pm i\alpha_1\sqrt{3})/2$, which are prohibited because $\mu f'(x_c) = \pm 1/\lambda'_{2,3}$ are not real. Then, $f'(x_c)$ takes positive and negative values at $\lambda_1 = 1$ and $\lambda_1 = -1$, respectively. The bifurcation points with $\lambda_1 = \pm 1$ are obtained from the condition

$$\mu f'(x_c) = \pm \frac{1}{\alpha_2 + \alpha_1}, \tag{47}$$

where the double-sign '±' corresponds to that of $\lambda_1 = \pm 1$.

To obtain the two remaining eigenvalues $\lambda_{2,3}$ at the bifurcation point with either $\lambda_1 = +1$ or -1, we substitute Eq. (47) into Eq. (45) and solve it into factors using $\lambda' - (\alpha_1 + \alpha_2) = 0$,

$$(\lambda' - (\alpha_1 + \alpha_2))((\alpha_1 + \alpha_2)^2\lambda'^2 - \alpha_2^2(2\alpha_2 + 3\alpha_1)\lambda' + \alpha_2^3(\alpha_2 + \alpha_1)) = 0. \tag{48}$$

Then, we obtain

$$\lambda'_{2,3} = \frac{1}{2(\alpha_1 + \alpha_2)^2}\Big[\alpha_2^2(2\alpha_2 + 3\alpha_1) \pm \sqrt{-\alpha_2^3\alpha_1^2(3\alpha_2 + 4\alpha_1)}\Big]. \tag{49}$$

The product $\lambda_2\lambda_3$ is given by

$$\lambda_2\lambda_3 = \mu^2 f'(x_c)^2 \lambda_2'\lambda_3' = \frac{\alpha_2^3}{(\alpha_2+\alpha_1)^3}. \tag{50}$$

For $\alpha_1 > -3\alpha_2/4$, $\lambda_{2,3}'$ given by Eq. (49) take nonreal complex conjugate values. From Eq. (50), $|\lambda_{2,3}| < 1$ for $\alpha_1 > 0$ and a bifurcation with either $\lambda_1 = 1$ or -1 may become the first bifurcation. Since $|\lambda_{2,3}| > 1$ for $-\alpha_2 < \alpha_1 < 0$, bifurcations with $\lambda_1 = \pm 1$ are not the first bifurcation and the first bifurcation should be a Hopf bifurcation.

To obtain Hopf bifurcations, we need to solve the cubic equation (45) and find two nonreal complex conjugate roots $\lambda_{2,3}'$ satisfying the condition $|\lambda_{2,3}| = 1$. It is not easy to find bifurcation points from the roots of the cubic equation, but we can find the condition that λ_2' and λ_3' are nonreal complex conjugate roots (see Appendix). The coefficients Q and R defined by Eq. (A·2) are represented as

$$\begin{aligned} Q &= -\frac{\mu^2 f'(x_c)^2\alpha_1^3}{9}[6\alpha_2 + \mu^2 f'(x_c)^2\alpha_1^3], \\ R &= \frac{\mu^2 f'(x_c)^2\alpha_1^3}{54}[27\alpha_2^2 + 18\alpha_2\alpha_1^3\mu^2 f'(x_c)^2 + 2\alpha_1^6\mu^4 f'(x_c)^4], \end{aligned} \tag{51}$$

and the coefficient D defined as $D = Q^3 + R^2$ is

$$D = \frac{1}{4}\alpha_1^6\alpha_2^4\mu^4 f'(x_c)^4 + \frac{1}{27}\alpha_1^9\alpha_2^3\mu^6 f'(x_c)^6. \tag{52}$$

As shown in Appendix, if $D > 0$, two nonreal complex conjugate roots exist. Since D takes a positive value for $\alpha_1 > 0$, λ_2 and λ_3 take nonreal complex conjugate values. Even for $\alpha_1 < 0$, if $|\alpha_1|$ and $|\mu f'(x_c)|$ are sufficiently small, nonreal complex conjugate roots exist.

3.2.4 3D map of $t_1/t_2 = 1/3$ including the function (2)

For $t_1/t_2 = 1/3$, the conditions for bifurcations with $\lambda_1 = \pm 1$ are given by Eq. (47). Combining Eq. (47) with Eq. (6), we obtain

$$2x_c^2 - 2x_0x_c \pm \Delta x^2 = 0, \tag{53}$$

where the double-sign '±' corresponds to that of $\lambda_1 = \pm 1$. For $\lambda_1 = 1$, the fixed point x_c at the bifurcation is given by

$$x_c = \frac{1}{2}\Big(x_0 \pm \sqrt{x_0^2 - 2\Delta x^2}\Big). \tag{54}$$

For $x_0 = 0.2$ and $\Delta x = 0.5$, the discriminant is negative and x_c takes a nonreal complex value. Thus, the pitchfork bifurcation with $\lambda_1 = 1$ is prohibited. For $\lambda_1 = -1$, the fixed point x_c is

given by

$$x_c = \frac{1}{2}\Big(x_0 \pm \sqrt{x_0^2 + 2\Delta x^2}\Big). \tag{55}$$

Since $x_c > x_0$ for $f'(x_c) < 0$, the root with a plus sign is selected and the period-doubling bifurcation with $\lambda_1 = -1$ occurs. At the bifurcation, x_c is independent of α_1, but, from Eq. (6), μ depends on α_1 as $\mu = \mu_1/(\alpha_1 + \alpha_2)$, where μ_1 indicates μ at the bifurcation for the single-delay system with $\alpha_1 = 0$ and $\alpha_2 = 1$.

From the discussion in Sect. 3.2.3, for $\alpha_1 > 0$, the first bifurcation is a period-doubling bifurcation, i.e., the bifurcation for the relevant condition, and a Hopf bifurcation may follow it. For $\alpha_1 < 0$, a Hopf bifurcation should occur in a physically important range of μ and should become the first bifurcation. A bifurcation with $\lambda = -1$ may follow it.

3.2.5 Map for the condition $t_1/t_2 = 2/3$

In the case of $t_1/t_2 = 2/3$, the map (3) is represented as

$$x_{j+1} = \mu\alpha_1 f(x_{j-1}) + \mu\alpha_2 f(x_{j-2}). \tag{56}$$

By introducing the variables $\xi_i = x_{3i}$, $\eta_i = x_{3i+1}$, and $\zeta_i = x_{3i+2}$, the map (56) is transformed to a 3D map:

$$\begin{aligned}
\xi_{i+1} &= \mu\alpha_1 f(\eta_i) + \mu\alpha_2 f(\xi_i), \\
\eta_{i+1} &= \mu\alpha_1 f(\zeta_i) + \mu\alpha_2 f(\eta_i), \\
\zeta_{i+1} &= \mu\alpha_1 f(\xi_{i+1}) + \mu\alpha_2 f(\zeta_i) \\
&= \mu\alpha_1 f(\mu\alpha_1 f(\eta_i) + \mu\alpha_2 f(\xi_i)) + \mu\alpha_2 f(\zeta_i).
\end{aligned} \tag{57}$$

The fixed point of the 3D map (57) (ξ_c, η_c, ζ_c) satisfies the following equations:

$$\begin{aligned}
\xi_c &= \mu\alpha_1 f(\eta_c) + \mu\alpha_2 f(\xi_c), \\
\eta_c &= \mu\alpha_1 f(\zeta_c) + \mu\alpha_2 f(\eta_c), \\
\zeta_c &= \mu\alpha_1 f(\xi_c) + \mu\alpha_2 f(\zeta_c).
\end{aligned} \tag{58}$$

The fixed point x_c of the two-to-one map (56) is the fixed point of the 3D map (57), i.e., $\xi_c = \eta_c = \zeta_c = x_c$. In the case that ξ_c, η_c, and ζ_c are different from each other, the fixed points are triplets, (ξ_c, η_c, ζ_c), (η_c, ζ_c, ξ_c), and (ζ_c, ξ_c, η_c), each of which is interpreted as a period-3 cycle for the two-to-one map (56).

To consider the stability of the fixed point (x_c, x_c, x_c), we introduce a variational equation

around the fixed point,

$$\begin{aligned}
\delta\xi_{i+1} &= \mu f'(x_c)(\alpha_1\delta\eta_i + \alpha_2\delta\xi_i),\\
\delta\eta_{i+1} &= \mu f'(x_c)(\alpha_1\delta\zeta_i + \alpha_2\delta\eta_i),\\
\delta\zeta_{i+1} &= \mu f'(x_c)(\alpha_1\delta\xi_{i+1} + \alpha_2\delta\zeta_i)\\
&= \mu f'(x_c)[\mu f'(x_c)\alpha_1\alpha_2\delta\xi_i + \mu f'(x_c)\alpha_1^2\delta\eta_i + \alpha_2\delta\zeta_i]. \qquad (59)
\end{aligned}$$

Thus, we need to obtain the eigenvalues λ of the matrix

$$C = \mu f'(x_c)\begin{pmatrix} \alpha_2 & \alpha_1 & 0\\ 0 & \alpha_2 & \alpha_1\\ \mu f'(x_c)\alpha_1\alpha_2 & \mu f'(x_c)\alpha_1^2 & \alpha_2 \end{pmatrix}. \qquad (60)$$

We introduce λ' defined by $\lambda = \mu f'(x_c)\lambda'$. Then, λ' is a root of the following characteristic polynomial,

$$\begin{vmatrix} \alpha_2 - \lambda' & \alpha_1 & 0\\ 0 & \alpha_2 - \lambda' & \alpha_1\\ \mu f'(x_c)\alpha_1\alpha_2 & \mu f'(x_c)\alpha_1^2 & \alpha_2 - \lambda' \end{vmatrix} = 0, \qquad (61)$$

which is reduced to

$$(\alpha_2 - \lambda')^3 + \mu f'(x_c)\alpha_1^3\alpha_2 - \mu f'(x_c)\alpha_1^3(\alpha_2 - \lambda') = (\alpha_2 - \lambda')^3 + \mu f'(x_c)\alpha_1^3\lambda' = 0. \qquad (62)$$

First, we consider bifurcations with $\lambda = \pm 1$, for which Eq. (62) is reduced to

$$(\alpha_2 - \lambda')^3 \pm \alpha_1^3 = 0, \qquad (63)$$

where the double-sign '±' corresponds to that of $\lambda = \pm 1$. Then, $\lambda'_1 = \alpha_2 \pm \alpha_1$ are solutions of Eq. (63) with plus and minus signs, and $f'(x_c)$ takes positive and negative values for $\lambda = +1$ and $\lambda = -1$, respectively:

$$\mu f'(x_c) = \pm\frac{1}{\alpha_2 \pm \alpha_1}. \qquad (64)$$

Note that at $\alpha_1 = \alpha_2$, the period-doubling bifurcation with $\lambda = -1$ is prohibited because the denominator of Eq. (64) with the minus sign is zero. Moreover note that the two remaining roots for Eq. (63) with plus and minus signs are $\lambda'_{2,3} = (2\alpha_2 - \alpha_1 \pm i\alpha_1\sqrt{3})/2$ and $\lambda'_{2,3} = (2\alpha_2 + \alpha_1 \pm i\alpha_1\sqrt{3})/2$, respectively. These roots $\lambda'_{2,3}$ are ignored because $\mu f'(x_c) = \pm 1/\lambda'_{2,3}$ are not real.

To obtain the two remaining eigenvalues $\lambda_{2,3}$ at the bifurcation point with either $\lambda_1 = +1$

or -1, we substitute Eq. (64) into Eq. (62) and obtain

$$\mp(\alpha_2 \pm \alpha_1)(\lambda'^3 - 3\alpha_2\lambda'^2 + 3\alpha_2^2\lambda' - \alpha_2^3) + \alpha_1^3\lambda' = 0, \tag{65}$$

which is factorized to

$$\mp(\alpha_2 \pm \alpha_1)\left[\lambda'^2 - (2\alpha_2 \mp \alpha_1)\lambda' + \frac{\alpha_2^3}{\alpha_2 \pm \alpha_1}\right][\lambda' - (\alpha_2 \pm \alpha_1)] = 0. \tag{66}$$

In Eqs.(65) and (66), the double signs are in the same order. Thus, the two remaining roots of Eq. (66) are obtained as

$$\begin{aligned} \lambda_2' &= \frac{1}{2}\left[2\alpha_2 \mp \alpha_1 + \sqrt{\frac{(\pm\alpha_1 - 3\alpha_2)\alpha_1^2}{\alpha_2 \pm \alpha_1}}\right], \\ \lambda_3' &= \frac{1}{2}\left[2\alpha_2 \mp \alpha_1 - \sqrt{\frac{(\pm\alpha_1 - 3\alpha_2)\alpha_1^2}{\alpha_2 \pm \alpha_1}}\right]. \end{aligned} \tag{67}$$

Then, λ_2 and λ_3 take nonreal complex conjugate values if $\pm\alpha_1 - 3\alpha_2 < 0$, and the product $\lambda_2\lambda_3$ is given as

$$\lambda_2\lambda_3 = \mu^2 f'(x_c)^2\lambda_2'\lambda_3' = \frac{\alpha_2^3}{(\alpha_2 \pm \alpha_1)^3}. \tag{68}$$

In the case of $\alpha_1 > 0$, if a bifurcation with $\lambda_1 = 1$ occurs, $|\lambda_{2,3}| < 1$ owing to Eq. (68) with a plus sign, and the solutions with λ_2 and λ_3 are stable, while $|\lambda_{2,3}| > 1$ at a bifurcation with $\lambda_1 = -1$ owing to Eq. (68) with a minus sign, and the solutions with λ_2 and λ_3 are unstable. Therefore, a bifurcation with $\lambda_1 = -1$ is not the first bifurcation, but a bifurcation with $\lambda_1 = 1$ is the first bifurcation, if it occurs. In the case of $\alpha_1 < 0$, $|\lambda_{2,3}| > 1$ at a bifurcation with $\lambda_1 = 1$, and the solutions with λ_2 and λ_3 are unstable, while $|\lambda_{2,3}| < 1$ at a bifurcation with $\lambda_1 = -1$, and the solutions with λ_2 and λ_3 are stable. Thus, a bifurcation with $\lambda_1 = 1$ is not the first bifurcation, but a bifurcation with $\lambda_1 = -1$ should be the first bifurcation if no Hopf bifurcation occurs in the range $f'(x_c) > 0$.

To discuss the Hopf bifurcation, we consider the roots of the cubic equation (62). For Eq. (62), the coefficients Q, R, and D defined in Appendix are given as

$$\begin{aligned} Q &= -\frac{1}{3}\mu f'(x_c)\alpha_1^3, \\ R &= \frac{1}{2}\mu f'(x_c)\alpha_1^3\alpha_2, \\ D &= Q^3 + R^2 = -\frac{1}{27}\mu^3 f'(x_c)^3\alpha_1^9 + \frac{1}{4}\mu^2 f'(x_c)^2\alpha_1^6\alpha_2^2. \end{aligned} \tag{69}$$

Therefore, for the case that $f'(x_c) > 0$ and $\alpha_1 < 0$, and for the case that $f'(x_c) < 0$ and $\alpha_1 > 0$, two nonreal complex conjugate roots exist due to $D > 0$, and a Hopf bifurcation may

be observed. Since $\mu f'(x_c) \sim O(1/\alpha_2)$ and $|\alpha_1| \leq \alpha_2$, even for the case that $f'(x_c) > 0$ and $\alpha_1 > 0$, and for the case that $f'(x_c) < 0$ and $\alpha_1 < 0$, the coefficient D takes a positive value in a physically important range of μ, and two nonreal complex conjugate roots exist, namely, a Hopf bifurcation may occur.

3.2.6 3D map of $t_1/t_2 = 2/3$ including the function (2)

Let us consider bifurcations with $\lambda_1 = \pm 1$. Combining Eq. (64) with Eq. (6) gives a quadratic equation of x_c,

$$\frac{2(x_c - x_0)x_c}{(\alpha_1 + \alpha_2)\Delta x^2} = \mp \frac{1}{\alpha_2 \pm \alpha_1}, \tag{70}$$

where the double signs correspond to that of $\lambda_1 = \pm 1$ in the same order.

Thus, for $\lambda_1 = 1$, Eq. (70) is reduced to

$$2x_c^2 - 2x_0 x_c + \Delta x^2 = 0, \tag{71}$$

and the discriminant $d = x_0^2 - 2\Delta x^2$ takes a negative value for $x_0 = 0.2$ and $\Delta x = 0.5$. Thus, x_c is not real and the bifurcation with $\lambda_1 = 1$ is prohibited. For $\lambda_1 = -1$, Eq. (70) is reduced to

$$2x_c^2 - 2x_0 x_c - \frac{\alpha_2 + \alpha_1}{\alpha_2 - \alpha_1}\Delta x^2 = 0, \tag{72}$$

and x_c at the bifurcation is given by

$$x_c = \frac{1}{2}\left(x_0 \pm \sqrt{x_0^2 + 2\bar{\alpha}\Delta x^2}\right), \tag{73}$$

where $\bar{\alpha} \equiv \frac{\alpha_2+\alpha_1}{\alpha_2-\alpha_1}$. Since $f'(x_c)$ takes a negative value at the bifurcation with $\lambda_1 = -1$, namely, Eq. (64) with minus signs, the bifurcation should occur in the range $x_c > x_0$ and the root with a plus sign is selected. Note that, at $\alpha_1 = \alpha_2$, the bifurcation with $\lambda_1 = -1$ is prohibited because $\bar{\alpha}$ becomes infinite.

From the discussion in Sect. 3.2.5, for $\alpha_1 > 0$, a bifurcation $\lambda_1 = -1$ is not the first bifurcation and a Hopf bifurcation with $|\lambda_{2,3}| = 1$ becomes the first bifurcation. A bifurcation with $\lambda_1 = -1$ may follow it. For $\alpha_1 < 0$, a bifurcation $\lambda_1 = -1$ becomes the first bifurcation of the relevant condition in the BBP regime, for which the bifurcation point is given by Eq. (64) with minus signs. As shown later, the first bifurcation is a Hopf bifurcation in the ABP regime.

4. Bifurcation Diagrams for the Nondispersive System with $f(x) = \exp(-(x-x_0)^2/\Delta x^2)$

In this section, we show numerically obtained bifurcation diagrams for the 2D and 3D maps (13), (40), and (57) including the mapping function $f(x)$ given by Eq. (2).

4.1 Two-delay system with two positive feedback loops

For the two-delay system with two positive feedback loops, the mode selection rule is governed by the normal bifurcation process (NBP), for which t_1/t_2 = odd/odd is the relevant condition and t_1/t_2 =even/odd and odd/even are the irrelevant conditions. Here, we focus on the cases of the relevant condition $t_1/t_2 = 1/3$ and the irrelevant conditions $t_1/t_2 = 2/3$ and $1/2$.

4.1.1 Relevant condition $t_1/t_2 = 1/3$

As discussed in Sect. 3.2.4, the pitchfork bifurcation with $\lambda = 1$ is prohibited. For $\alpha_1 > 0$, the first bifurcation is a period-doubling bifurcation with $\lambda = -1$. A Hopf bifurcation should be the second bifurcation, if it occurs. Figures 5(a) and 5(b) show bifurcation diagrams for the maps (12), (39), and (56) with $\alpha_1/\alpha_2 = 1/2$ and $\alpha_1/\alpha_2 = 1$, respectively. The bifurcation diagrams colored red are those for the map (39). A bifurcation diagram of the map (39) is regarded as a projection of that of the 3D map (40) on the coordinate ξ. Period-doubling bifurcations occur at $\mu \approx 0.415$ and $\mu \approx 0.311$ for $\alpha_1/\alpha_2 = 1/2$ and $\alpha_1/\alpha_2 = 1$, respectively. Figure 6 shows the attractors of the 3D map (40) with $\alpha_1/\alpha_2 = 1/2$. At $\mu = 0.4$ before the first bifurcation, the fixed point (x_c, x_c, x_c) is the only attractor, but at $\mu = 0.5$ and 0.7, period-2 cycles generated by the period-doubling bifurcation with $\lambda = -1$ are observed.

Figure 7 shows the bifurcation of the fixed point together with the eigenvalues λ_i for the maps (13), (40), and (57). The red circle '$\circ$' indicates the bifurcation points of the 3D map (40). For the case $\alpha_1/\alpha_2 = 1/2$ in Fig. 7(a), the fixed point becomes a saddle-focus point after the first bifurcation with $\lambda = -1$. A Hopf bifurcation occurs as the second bifurcation; thus, the fixed point is finally unstable with $|\lambda_i| > 1$ ($i = 1, 2, 3$). As shown in Fig. 7(b), the second bifurcation does not occur for $\alpha_1/\alpha_2 = 1$. Indeed, it is numerically confirmed that in the limit of $\alpha_1 \to \alpha_2$, the second bifurcation point diverges as $\mu \propto \exp(\sqrt{1/\Delta\alpha_r})$, where $\Delta\alpha_r \equiv 1 - \alpha_1/\alpha_2$. Note that the existence of the second bifurcation of the fixed point does not disturb the period-2 cycle generated by the first bifurcation.

4.1.2 Irrelevant condition $t_1/t_2 = 2/3$

From the discussion in Sect. 3.2.6, for $\alpha_1 > 0$, the bifurcation with $\lambda = 1$ is prohibited and the first bifurcation is not a bifurcation with $\lambda = -1$. Thus, a Hopf bifurcation becomes the first bifurcation. In Figs. 5(a) and 5(b), the bifurcation diagrams of the map (56) are colored green. Hopf bifurcations occur at $\mu \approx 0.467$ and $\mu \approx 0.366$ for $\alpha_1/\alpha_2 = 1/2$ and $\alpha_1/\alpha_2 = 1$, respectively. Figures 8(a) and 8(b) show the attractors of the 3D map (57) with

(a)

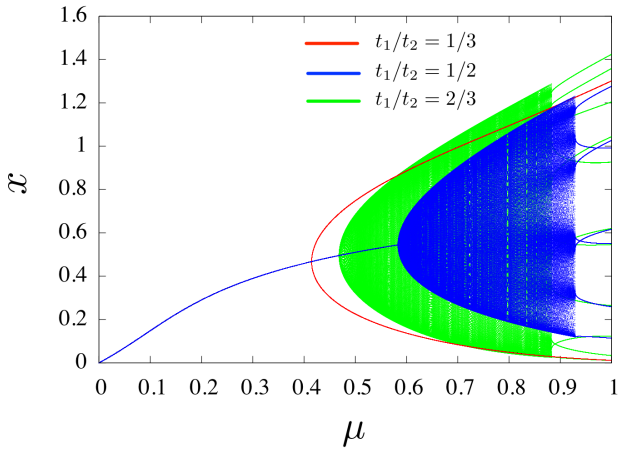

(b)

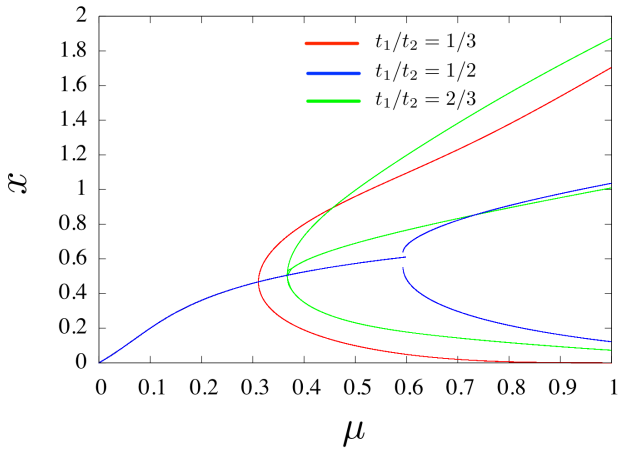

Fig. 5. (Color online) Bifurcation diagrams for the map (9) in the NBP regime. The three bifurcation diagrams of $t_1/t_2 = 1/3$, $1/2$, and $2/3$ are superposed on the same plane. The fixed point x_c is the same for the three bifurcation diagrams when α_1/α_2 is fixed. (a) $\alpha_1/\alpha_2 = 1/2$. (b) $\alpha_1/\alpha_2 = 1$.

$\alpha_1/\alpha_2 = 1/2$ and $\alpha_1/\alpha_2 = 1$, respectively. For $\alpha_1/\alpha_2 = 1/2$, quasiperiodic motion with an irrational rotation number on a torus seems to be excited by the Hopf bifurcation, and it changes to locking motion with period 11, namely, a period-11 cycle, at $\mu = 0.9$ [see Fig. 8(a)]. For $\alpha_1/\alpha_2 = 1$, the Hopf bifurcation generates locking motion, which forms a period-5 cycle as an attractor of the 3D map (57) [see Fig. 8(b)]. However, it appears as a period-3 cycle in its projection on the x-coordinate in Fig. 5(b) due to the degeneracy of the mapping points of the period-5 cycle.

In Fig. 7, the green square '□' indicates the bifurcation points of the 3D map (57). For the case $\alpha_1/\alpha_2 = 1/2$ in Fig. 7(a), the fixed point becomes a saddle-focus point after the first bifurcation, i.e., the Hopf bifurcation. The second bifurcation is a bifurcation with $\lambda = -1$

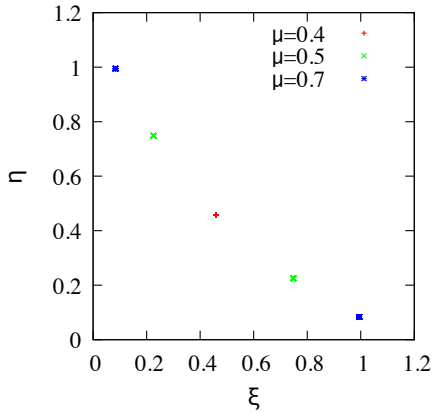

Fig. 6. (Color online) Attractors of the 3D map (40) with $\alpha_1/\alpha_2 = 1/2$. Three attractors at $\mu = 0.4$, 0.5, and 0.7 are superposed on the projection plane (ξ, η).

and the fixed point becomes unstable with $|\lambda_i| > 1$ $(i = 1, 2, 3)$. For the case $\alpha_1/\alpha_2 = 1$ in Fig. 7(b), the second bifurcation does not occur because the bifurcation with $\lambda = -1$ is prohibited as pointed out in Sect. 3.2.5. Indeed, in the limit of $\alpha_1 \to \alpha_2$, the second bifurcation point diverges as $\mu \propto \Delta\alpha_r^{-1/2} \exp(1/\Delta\alpha_r)$ from Eqs. (5) and (73).

4.1.3 Irrelevant condition $t_1/t_2 = 1/2$

From the discussion in Sect. 3.2.2, only the Hopf bifurcation occurs in this case. In Fig. 5, the bifurcation diagrams of the map (12) are colored blue. As shown in Fig. 5(a), a Hopf bifurcation occurs at $\mu \approx 0.583$ for $\alpha_1/\alpha_2 = 1/2$. For the case $\alpha_1/\alpha_2 = 1$ in Fig. 5(b), it seems as if a period-doubling bifurcation occurs at $\mu \approx 0.597$. However, as shown in Fig. 9, a period-3 cycle is really generated as an attractor of the 2D map (13), which is theoretically predicted from Eq. (29). Furthermore, the bifurcation is not supercritical but subcritical.[24,25] Indeed, there exist two attractors, i.e., the fixed point (x_c, x_c) and period-3 cycle, in the range $0.593 < \mu < 0.597$; for example, see the attractors at $\mu = 0.595$ in Fig. 9. In Fig. 7, the blue diamond '$\diamond$' indicates the bifurcation points of the 2D map (13). A Hopf bifurcation is the first bifurcation and there is no second bifurcation.

4.1.4 Common structure of the bifurcation diagrams for the two-delay system with two positive feedback loops

As a result of the theoretical and numerical analyses, there is a common structure of the bifurcation diagrams for the two-delay system with two positive feedback loops, as schematically shown in Fig. 10. At the first bifurcation, a period-doubling bifurcation with $\lambda = -1$ occurs for the relevant condition but Hopf bifurcations take place for the irrelevant conditions.

(a)

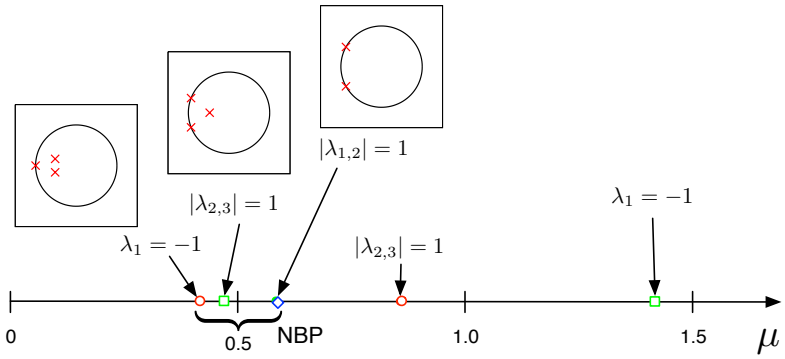

(b)

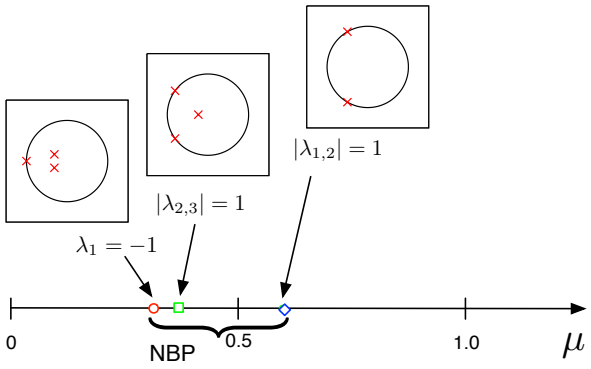

Fig. 7. (Color online) Bifurcation of the fixed point together with the eigenvalues λ_i for the maps (13), (40), and (57) in the NBP regime. The red circle '$\circ$', blue diamond '$\diamond$', and green square '$\square$' indicate the bifurcation points for $t_1/t_2 = 1/3$, $1/2$, and $2/3$, respectively. The label 'NBP' indicates the first bifurcations governed by NBP. At each bifurcation point of NBP, the inset shows the eigenvalues λ_i in comparison with the unit circle in the complex plane. (a) $\alpha_1/\alpha_2 = 1/2$. (b) $\alpha_1/\alpha_2 = 1$.

As shown in Fig. 7, the bifurcation point for the relevant condition is smaller in μ than those for the irrelevant conditions. This corresponds to the fact that the relevant condition takes the largest value in $\bar{\eta}$ $(= \mu f'(x_c))$ at the first bifurcation, which is confirmed by the linear stability analysis.[18,20] The second bifurcations are observed for the 3D maps in the range $0 < \alpha_1 < \alpha_2$ and no second bifurcation occurs at $\alpha_1 = \alpha_2$.

4.2 Two-delay system with positive and negative feedback loops

Here, we concentrate on the cases of $t_1/t_2 = 1/2$ and $2/3$ because the rate $t_1/t_2 = 1/3$ is irrelevant for both BBP and ABP, and we can study the relevant and irrelevant conditions in the BBP and ABP regimes taking the two cases $t_1/t_2 = 1/2$ and $2/3$ into account. For the two-delay system with positive and negative feedback loops, the mode selection rule changes with α_1. At $t_1/t_2 = 1/2$, i.e., the relevant condition of ABP, the threshold between BBP and

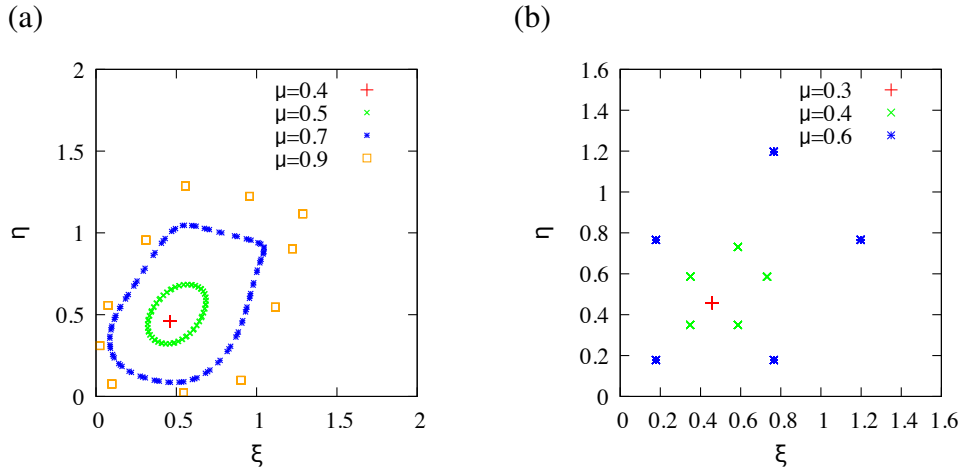

Fig. 8. (Color online) Attractors at representative values of μ of the 3D map (57) in the NBP regime, which are superposed on the projection plane (ξ, η). (a) $\alpha_1/\alpha_2 = 1/2$. (b) $\alpha_1/\alpha_2 = 1$.

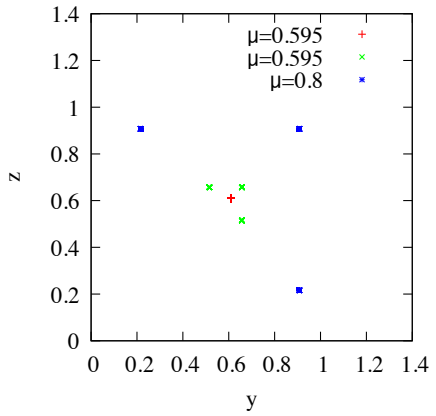

Fig. 9. (Color online) Attractors at representative values of μ of the 2D map (13) with $\alpha_1/\alpha_2 = 1$.

ABP, α_{th}, is defined by Eq. (35) and takes a value of $-\frac{23}{27}\alpha_2 \approx -0.851851\alpha_2$ for $x_0 = 0.2$ and $\Delta x = 0.5$. As will be discussed in this subsection, at $t_1/t_2 = 2/3$, i.e., the irrelevant condition of ABP, the threshold is slightly smaller than α_{th}. Generally, the thresholds for irrelevant conditions of ABP seem to be slightly smaller than α_{th}. Then, if α_1 is larger than α_{th}, BBP governs the mode selection rule. There is a small range below α_{th} in which the bifurcation obeys either BBP or ABP depending on the rate t_1/t_2, namely, the mixed regime of BBP and ABP. If α_1 is below this range, ABP dominates the mode selection rule. In the following, we numerically study the properties of the 2D map (13) and 3D map (57) with $\alpha_1/\alpha_2 = -1/2$ in the BBP regime and with $\alpha_1/\alpha_2 = -0.9$ in the ABP regime.

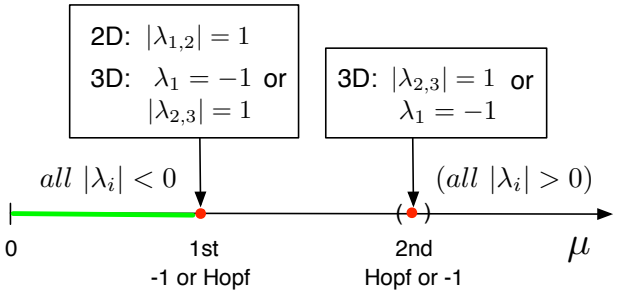

Fig. 10. (Color online) Bifurcation process of the fixed point in the NBP regime. On the thick green line, the fixed point is stable. The bifurcation in the parentheses $(\cdots)$ does not occur for the 3D maps with $\alpha_1 = \alpha_2$ and for the 2D map.

4.2.1 $t_1/t_2 = 2/3$: relevant condition for BBP and irrelevant condition for ABP

The rate $t_1/t_2 = 2/3$ is relevant for BBP and irrelevant for ABP. It is numerically shown that the threshold between BBP and ABP, $\alpha_{th2/3}(< \alpha_{th})$, is in the range $-0.878 < \alpha_{th2/3}/\alpha_2 < -0.877$ for $x_0 = 0.2$ and $\Delta x = 0.5$. From the discussion in Sect. 3.2.6, for $-\alpha_2 < \alpha_1 < 0$, the bifurcation with $\lambda = 1$ is prohibited and a period-doubling bifurcation with $\lambda = -1$ occurs in the range $f'(x_c) < 0$, i.e., $x_c > x_0$.

• BBP regime at $\alpha_1/\alpha_2 = -1/2$

Figure 11 shows the bifurcation diagram of the map (56) with $\alpha_1/\alpha_2 = -1/2$ and Fig. 12 shows the attractors of the 3D map (57) with $\alpha_1/\alpha_2 = -1/2$. A period-doubling bifurcation at $\mu \approx 0.698$ generates a period-2 cycle, and with increasing μ, it bifurcates into a pair of circles [see Fig. 12(a)]. Furthermore, the attractor undergoes some bifurcations and changes to a chaotic attractor [see Fig. 12(b)]. Although it is out of the range of Fig. 11, the chaotic attractor finally changes to a stable attractor, a period-7 cycle, at $\mu \approx 1.321$.

Figure 13 shows the bifurcation of the fixed point together with the eigenvalues λ_i for the 2D map (13) and 3D map (57) with $\alpha_1/\alpha_2 = -1/2$. The green square '□' indicates the bifurcation points of the fixed point of the 3D map (57). As discussed in Sect. 3.2.6, if the first bifurcation does not occur in the range $f'(x_c) > 0$, a period-doubling bifurcation becomes the first bifurcation. In this case, a Hopf bifurcation occurs as the second bifurcation, which may have an effect on the creation of the chaotic attractor.

• ABP regime at $\alpha_1/\alpha_2 = -0.9$

First note that, from Eqs.(5) and (6) with $x_0 = 0.2$ and $\Delta x = 0.5$, $x_c = 0.2$ and $f'(x_c) = 0$ at $\mu = 2$ for $\alpha_1/\alpha_2 = -0.9$, and $f'(x_c)$ takes positive and negative values in the ranges $0 < \mu < 2$ and $\mu > 2$, respectively. That is, the bifurcation governed by ABP occurs in the range $0 < \mu < 2$ and that governed by BBP arises in the range $\mu > 2$. As shown in Fig. 14,

the first bifurcation of the fixed point x_c is a Hopf bifurcation at $\mu \approx 0.611$ (see the set of blue points labeled 'D1'). For the 3D map (57), a circle attractor is created by the Hopf bifurcation [see Fig. 15(a)]. However, the circle attractor suddenly disappears owing to a subcritical-like bifurcation at $\mu \approx 0.787$ and motion is transferred to a new attractor, which is formed by triplets of period-4 cycles [see Fig. 15(a)]. We call the new attractor the outer attractor (the set of red points labeled 'D2' in Fig. 14). The outer attractor undergoes some bifurcations and changes to a chaotic attractor at $\mu \approx 0.8$. Actually, it consists of forty-eight chaotic islands at $\mu = 0.8$ [see Fig. 15(a)], which are merged into a large chaotic attractor with increasing μ [see Fig. 15(b)]. Finally, it changes to a period-7 cycle at $\mu \approx 1.254$ [see the red crosses '$\times$' in Fig. 15(c)]. As shown in Fig. 14, the outer attractor arises as triplets of fixed points at $\mu \approx 0.626$ (see the discussion on the fixed points in Sect. 3.2.5). With increasing μ, each fixed point undergoes period-doubling bifurcations twice and the triplets of the fixed points change to the triplets of period-4 cycles at $\mu \approx 0.757$.

In Fig. 14, a subdominant attractor (see the set of green points labeled 'S') exists in the range $1.387 < \mu < 2.342$ and it is generated under the influence of the second and third bifurcations of the fixed point. At both ends, the subdominant attractor ceases to exist owing to subcritical-like bifurcations. Figure 16 shows the bifurcation of the fixed point together with the eigenvalues λ_i for the 2D map (13) and 3D map (57) with $\alpha_1/\alpha_2 = -0.9$. The green square '$\square$' indicates the bifurcation points of the fixed point of the 3D map (57). There are four bifurcation points. Since $f'(x_c) > 0$ in the range $0 < \mu < 2$, the first and second bifurcations are Hopf bifurcations in the ABP regime and have the same set of eigenvalues λ_i ($i = 1, 2, 3$). Since the roots of the cubic equation (62) depend only on $\mu f'(x_c)$ when α_1 and α_2 are fixed, $\mu f'(x_c)$ should take the same value at the first and second bifurcation points. In the range $0 < \mu < 2$, $\mu f'(x_c)$ first increases from zero, takes the maximum at a certain point, and decreases to zero; thus $\mu f'(x_c)$ takes the same value twice in the range $0 < \mu < 2$ except the maximum. As a result, if ABP takes place, the fixed point changes from a stable point to a saddle-focus point at the first bifurcation and undergoes the reverse process at the second bifurcation. The third and fourth bifurcations occur in the range $\mu > 2$, i.e., $f'(x_c) < 0$. Since $t_1/t_2 = 2/3$ is a relevant condition in the BBP regime, the third bifurcation is a period-doubling bifurcation, and a Hopf bifurcation, i.e., the fourth bifurcation, follows. Therefore, the fixed point is stabilized between the second and third bifurcations [see the green cross '+' in Fig. 15(c)] and a subdominant attractor appears in a range including the interval between the second and third bifurcation points. As shown in the insets of Fig. 14, oscillations induced by the Hopf bifurcation are observed before the second bifurcation and

the bifurcation diagram after the third bifurcation is similar to that in Fig. 11.

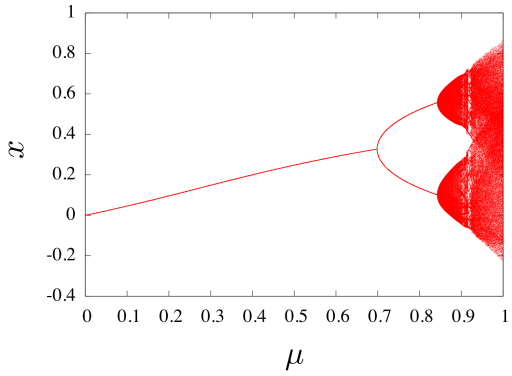

Fig. 11. (Color online) Bifurcation diagram of the map (56) with $\alpha_1/\alpha_2 = -1/2$.

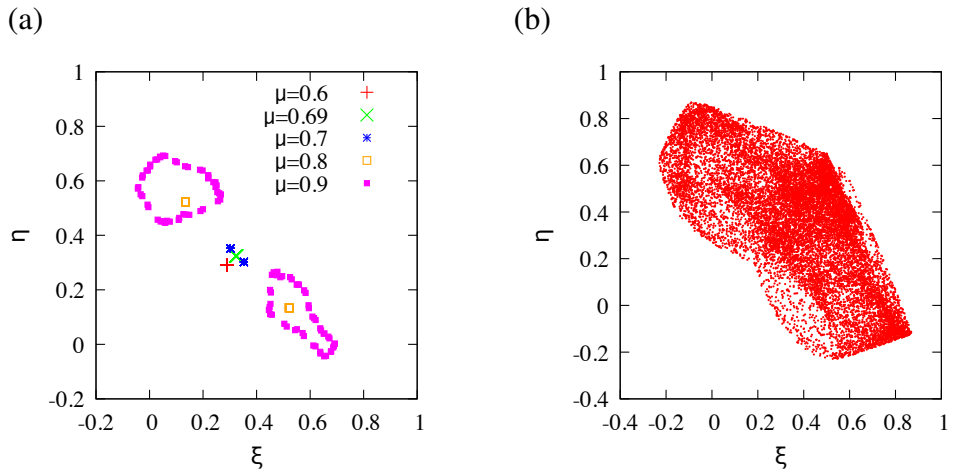

Fig. 12. (Color online) Attractors of the 3D map (57) with $\alpha_1/\alpha_2 = -1/2$. (a) Regular attractors at representative values of μ. (b) Chaotic attactor at $\mu = 1.0$.

4.2.2 $t_1/t_2 = 1/2$: irrelevant condition for BBP and relevant condition for ABP

The rate $t_1/t_2 = 1/2$ is irrelevant for BBP and relevant for ABP. The threshold between BBP and ABP, α_{th}, defined by Eq. (35) takes a value of $-\frac{23}{27}\alpha_2 \approx -0.851\alpha_2$. From the discussion in Sect. 3.2.2, the bifurcation with $\lambda = -1$ is prohibited and the bifurcation with $\lambda = 1$ is allowed in the range $f'(x_c) > 0$, i.e., $x_c < x_0$.

• BBP regime at $\alpha_1/\alpha_2 = -1/2$

Figure 17 shows the bifurcation diagram of the map (12) with $\alpha_1/\alpha_2 = -1/2$. First, a Hopf bifurcation occurs at $\mu \approx 0.828$ and a quasiperiodic oscillation is created. However, the attractor

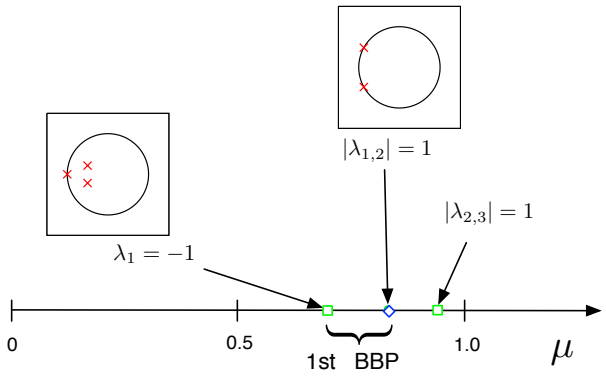

Fig. 13. (Color online) Bifurcation of the fixed point together with the eigenvalues λ_i for the maps (13) and (57) with $\alpha_1/\alpha_2 = -1/2$. The blue diamond '◇' and green square '□' indicate the bifurcation points of $t_1/t_2 = 1/2$ and $2/3$, respectively. The label 'BBP' indicates the first bifurcations governed by BBP. At each bifurcation point of BBP, the inset shows the eigenvalues λ_i in comparison with the unit circle in the complex plane.

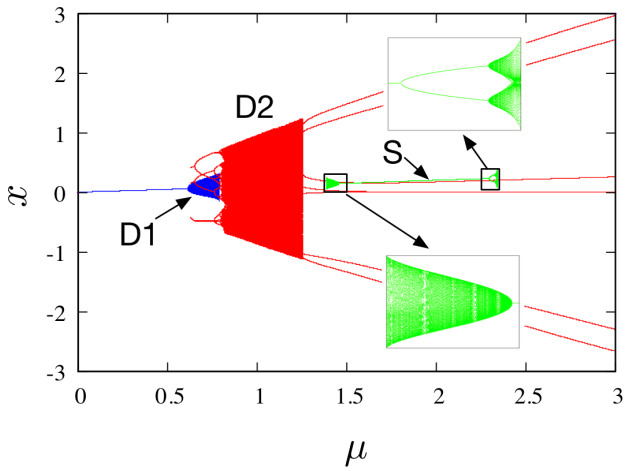

Fig. 14. (Color online) Bifurcation diagram of the map (56) with $\alpha_1/\alpha_2 = -0.9$. The fixed point x_c before the first bifurcation and the attractor generated by it, i.e., the set of blue points, are labeled 'D1'. The outer attractor, i.e., the set of red points, is labeled 'D2'. The attractor labeled 'S', i.e., the set of green points, is the subdominant attractor, whose enlarged views near the upper and lower ends are shown in the insets.

changes to a pair of period-5 cycles at $\mu \approx 0.989$ and further changes to a chaotic attractor at $\mu \approx 1.032$ after some bifurcations. Finally, the chaotic attractor changes to a stable attractor, a period-3 cycle, at $\mu \approx 1.192$.

In Fig. 13, the blue diamond '◇' indicates the bifurcation points of the fixed point of the 2D map (13) with $\alpha_1/\alpha_2 = -1/2$. As discussed in Sect. 3.2.2, since the first bifurcation does not occur in the range $f'(x_c) > 0$, a Hopf bifurcation in the range $f'(x_c) < 0$ becomes the first bifurcation and no bifurcation follows it.

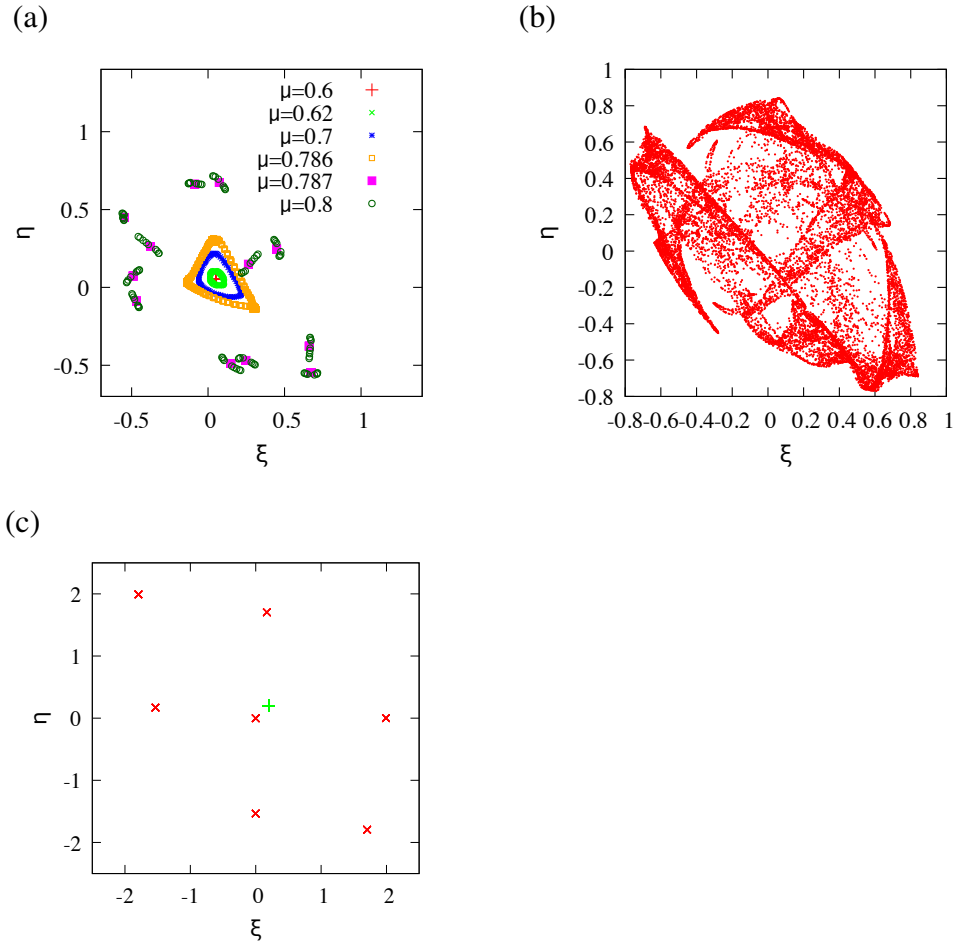

Fig. 15. (Color online) Attractors of the 3D map (57) with $\alpha_1/\alpha_2 = -0.9$. (a) Regular and chaotic attractors at representative values of μ. Forty-eight chaotic islands are observed at $\mu = 0.8$. (b) Chaotic attractor at $\mu = 0.9$. (c) Attractors at $\mu = 2$. The dominant attractor forms a period-7 cycle (the red crosses '×') and the subdominant attractor is the fixed point (the green cross '+').

• ABP regime at $\alpha_1/\alpha_2 = -0.9$

As shown in Fig. 18, the first bifurcation occurs in the range $0 < \mu < 2$ and is a pitchfork bifurcation (see the set of red points labeled 'D', i.e., the dominant attractor). For the 2D map (13) in Fig. 19(a), a pair of stable fixed points is generated by the pitchfork bifurcation of the fixed point (x_c, x_c) at $\mu \approx 0.459$ and, with increasing μ, each of the paired fixed points undergoes a period-doubling cascade, changing to a chaotic attractor at $\mu \approx 0.802$. Furthermore, the paired chaotic attractors are unified to one chaotic attractor [see Fig. 19(b)]. Finally, it changes to a period-7 cycle at $\mu \approx 1.374$ [see the red crosses '×' in Fig. 19(c)].

In Fig. 18, a subdominant attractor (see the set of green points labeled 'S') exists in the range $1.595 < \mu < 2.692$ and is generated under the influence of the second and third bifurcations of the fixed point x_c. Between these bifurcations, the fixed point is stable [see the

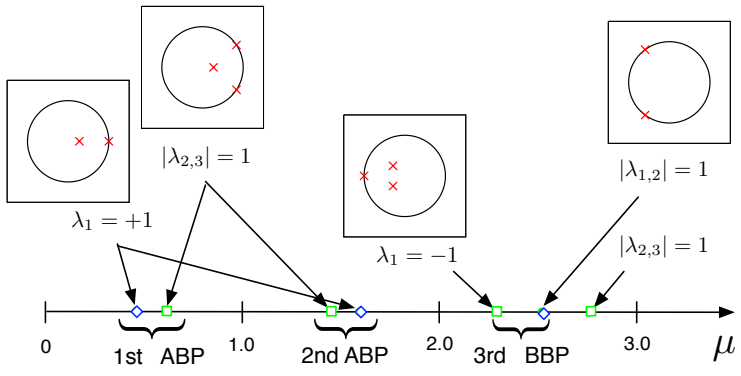

Fig. 16. (Color online) Bifurcation of the fixed point together with the eigenvalues λ_i for the maps (13) and (57) with $\alpha_1/\alpha_2 = -0.9$. The blue diamond '◇' and green square '□' indicate the bifurcation points of $t_1/t_2 = 1/2$ and $2/3$, respectively. At each bifurcation point of ABP and BBP, the inset shows the eigenvalues λ_i in comparison with the unit circle in the complex plane.

green cross '+' in Fig. 19(c)]. In Fig. 16, the blue diamond '◇' indicates the bifurcation points of the fixed point of the 2D map (13). There are three bifurcation points. The first and second bifurcations are bifurcations with $\lambda = 1$ in the ABP regime $0 < \mu < 2$, namely, $f'(x_c) > 0$, and they have the same set of eigenvalues λ_1 and λ_2 for the reason explained in Sect. 4.2.1. The first bifurcation is a supercritical pitchfork bifurcation and a pair of fixed points appears after the bifurcation. However, the second bifurcation is a subcritical pitchfork bifurcation and solutions with weak instability are observed.[24,25] Indeed, as shown in the lower inset of Fig. 18, in a range just below the second bifurcation point, a solution starting from a point very close to the fixed point x_c stays in its neighborhood for an exponentially long time. On the other hand, the third bifurcation occurs in the BBP regime $\mu > 2$ and it is a supercritical Hopf bifurcation because $t_1/t_2 = 1/2$ is an irrelevant condition in the BBP regime. As shown in the upper inset of Fig. 18, a small attractor induced by the third bifurcation exists, whose bifurcation diagram is similar to that in Fig. 17.

4.2.3 Common structure of the bifurcation diagrams in the BBP regime

A common structure of the bifurcation diagrams in the BBP regime exists. The bifurcation process of the fixed point is similar to that in the NBP regime in Fig. 10. At the first bifurcation, a period-doubling bifurcation with $\lambda = -1$ occurs for the relevant condition but a Hopf bifurcation takes place for the irrelevant condition. As shown in Fig. 13, the period-doubling bifurcation for the relevant condition appears at a smaller value of μ than the Hopf bifurcation for the irrelevant condition. This corresponds to the fact that the relevant condition takes the largest value in $\bar{\eta}$ $(= \mu f'(x_c))$ at the first bifurcation, which is predicted by

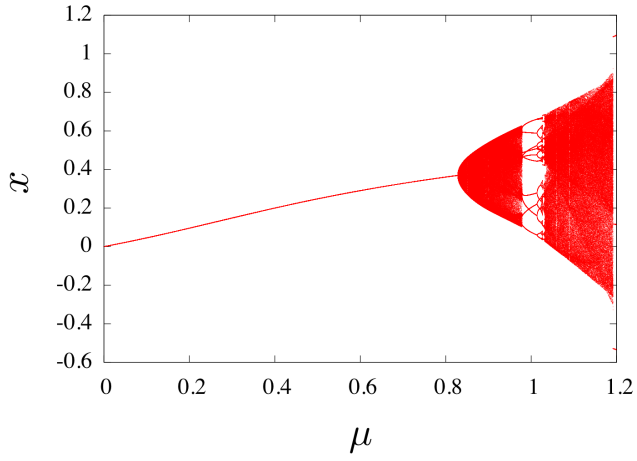

Fig. 17. (Color online) Bifurcation diagram of the map (12) with $\alpha_1/\alpha_2 = -1/2$.

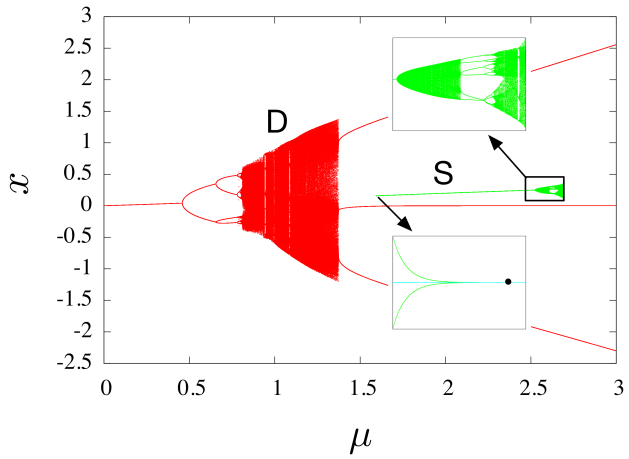

Fig. 18. (Color online) Bifurcation diagram of the map (12) with $\alpha_1/\alpha_2 = -0.9$. The dominant and subdominant attractors, i.e., the set of red points and the set of green points, are labeled 'D' and 'S', respectively. In the upper inset, an enlarged bifurcation diagram near the upper end of the subdominant attractor is shown. In the lower inset, a set of initial points close to the fixed points (cyan) and mapped points after 10^5 iterations (green) are shown in a very small area ($1.595853 \leq \mu \leq 1.59586,\ 0.1581 \leq x \leq 0.1589$), and the black bullet is the bifurcation point of the fixed point.

linear stability analysis.[18,20] The second bifurcation is observed only for the 3D map. Note that for the irrelevant condition $t_1/t_2 = 1/3$, the first bifurcation is a Hopf bifurcation and a bifurcation with $\lambda = -1$ arises as the second bifurcation.

The attractors induced by BBP undergo some bifurcations with increasing μ. For the irrelevant condition, an oscillation with an irrational rotation number is excited at the first bifurcation; it changes to locking motion, and it further bifurcates to a chaotic attractor. It

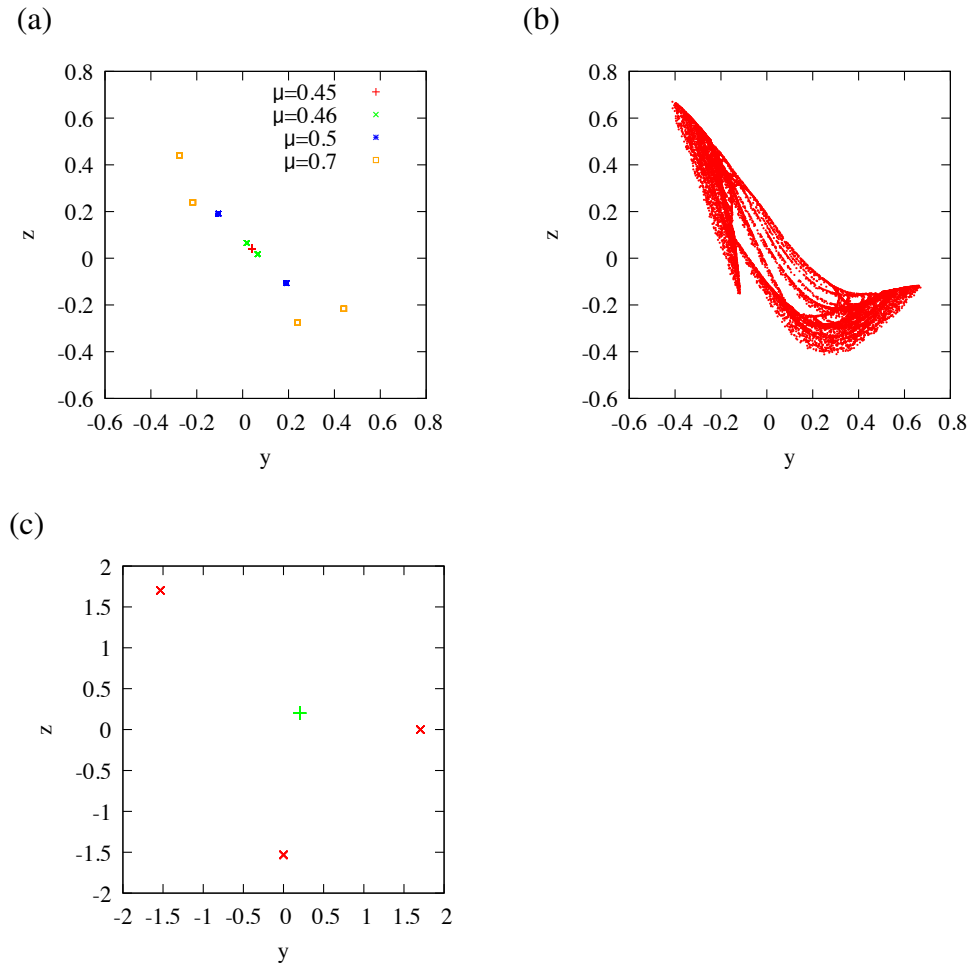

Fig. 19. (Color online) Attractors of the 2D map (13) with $\alpha_1/\alpha_2 = -0.9$. (a) Regular attractors at representative values of μ. (b) Chaotic attactor at $\mu = 0.85$. (c) Attractors at $\mu = 2$. The dominant attractor forms a period-3 cycle (the red crosses '×') and the subdominant attractor is the fixed point (the green cross '+').

finally changes to locking motion. For the relevant condition, a period-2 cycle is excited by the first bifurcation; it changes to twin circles with an irrational rotation number, and a unified chaotic attractor appears through subsequent bifurcations. It finally changes to locking motion.

4.2.4 Common structure of the bifurcation diagrams in the ABP regime

The common structure of the bifurcation diagrams in the ABP regime is schematically shown in Fig. 20, in which we include the result for the case of $t_1/t_2 = 1/3$. For each of the relevant and irrelevant conditions, the first and second bifurcations are observed in the ABP regime, i.e., $f'(x_c) > 0$, and have the same set of eigenvalues. This is because the eigenvalues λ_i are determined by $\mu f'(x_c)$ if α_1 and α_2 are fixed [see Eqs.(18), (45), and (62)], and $\mu f'(x_c)$ takes the same value at the first and second bifurcation points, as discussed in Sects. 4.2.1

and 4.2.2. As a result, the fixed point changes from a stable point to a saddle (saddle-focus) point at the first bifurcation and undergoes the reverse process at the second bifurcation.

As shown in Fig. 16, the first and second bifurcations for the relevant condition in the ABP regime are pitchfork bifurcations with $\lambda = 1$, but those for the irrelevant conditions are Hopf bifurcations. Note that the second bifurcation for the relevant condition is a subcritical pitchfork bifurcation.[24] The first and second bifurcations for the relevant condition occur at smaller and larger values of μ than those for the irrelevant conditions, respectively.

The third bifurcations are induced by BBP and their properties are essentially the same as the first bifurcations in the BBP regime. Note that the fourth bifurcation does not appear for the 2D map, i.e., $t_1/t_2 = 1/2$.

For the relevant condition of ABP, the attractor generated by the first bifurcation, the dominant attractor, always exists for the range above the first bifurcation. However, for each irrelevant condition of ABP, the attractor caused by the first bifurcation soon disappears owing to a subcritical-like bifurcation, and motion is transferred to the outer attractor, which exists in a large range of μ and is regarded as the dominant attractor. For each of the relevant and irrelevant conditions, the fixed point is stable between the second and third bifurcations, and the subdominant attractor exists in a finite range, which includes the second and third bifurcation points. In a small range above the third bifurcation, the bifurcation diagram of the subdominant attractor is similar to that observed in the BBP regime. On the other hand, in a range below the second bifurcation, the attractor created by a Hopf bifurcation is observed for each irrelevant condition, but solutions with weak instability due to the subcritical pitchfork bifurcation are observed for the relevant condition.

As a result, the attractors generated by the first bifurcations for the relevant and irrelevant conditions and the outer attractors for the irrelevant conditions are regarded as objects in the ABP regime. Let us call these attractors in the ABP regime the dominant attractors. However, oscillations governed by BBP still survive in limited ranges, and they are hidden by the dominant attractors created by ABP. Thus, the subdominant attractors make their appearance as intermediate objects governed by both ABP and BBP.

5. Bifurcation Diagrams for the Dispersive System with $\gamma = 210$

5.1 Relation between solutions of the nondispersive and dispersive systems

In this section, we discuss the numerical results of the dispersive system with $\gamma = 210$ in comparison with those of the nondispersive system in Sect. 4. First, we consider the relationship between the solutions of the nondispersive and dispersive systems.

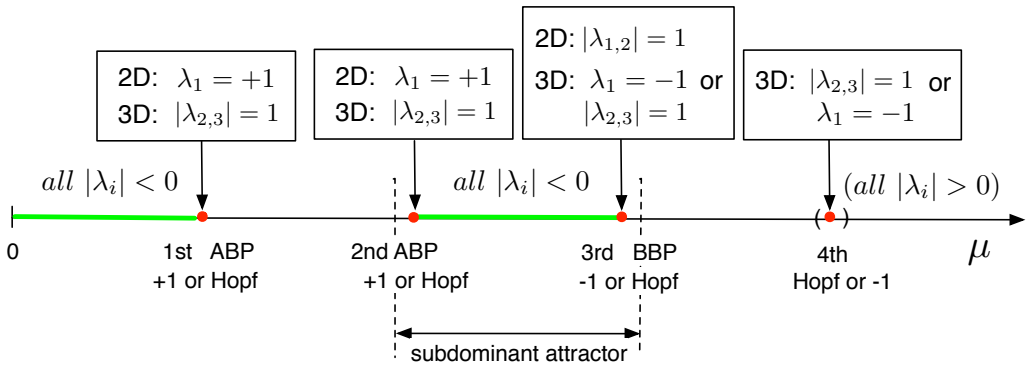

Fig. 20. (Color online) Bifurcation process of the fixed point in the ABP regime combined with the BBP regime. On the thick green lines, the fixed point is stable. The bifurcation point in the parentheses $(\cdots)$ does not occur for the 2D map.

The solutions of the nondispersive system obey the following rules.

R1: If a sequence $(x_0, x_1, x_2, \cdots, x_{n-1}, x_n, x_{n+1}, \cdots)$ is a solution of the two-to-one map (9), a sequence generated by applying a shift operator $x_n \to x_{n-1}$ on it, i.e., $(x_1, x_2, \cdots, x_{n-1}, x_n, x_{n+1}, \cdots)$, is a solution.

R2: For a stable period-l cycle for the m-dimensional map (11) defined by $\boldsymbol{X} = \boldsymbol{F}^l(\boldsymbol{X})$, there exists a nonperiodic sequence with length l, i.e., $(x_0, x_1, \cdots, x_{l-1})$, and the period-$l$ cycle is represented by the repetition of the sequence m times if $1 < l$, m/l is an irreducible fraction, and no other stable period-l cycle exists. Namely, a stable period-l cycle $(x_0, x_1, \cdots, x_{l-1})$ exists for the two-to-one map (9), and, from the definition (10), the period-l cycle $(\boldsymbol{X}_0, \boldsymbol{X}_1, \cdots, \boldsymbol{X}_{l-1})$ is given by $(x_0, x_1, \cdots, x_{l-1}, x_l(= x_0), x_{l+1}(= x_1), \cdots, x_{ml-1}(= x_{l-1}))$. Any subsequence with length m in $(x_0, x_1, \cdots, x_{l-1}, x_l, x_{l+1}, \cdots)$, i.e., $(x_k, \cdots, x_{k+m-1})$ $(0 \le k \le l-1)$, corresponds to one of the points of the stable period-l cycle for the m-dimensional map due to item **R1**.

The item **R1** is immediately obtained from the definition of the map (9). The item **R2** is a conjecture based on the numerical evidence combined with the item **R1**. Examples are as follows.

E1: For the 1D map (4), a period-doubling bifurcation generates a period-2 cycle ($m = 1$, $l = 2$), which is represented as $(\boldsymbol{X}_1, \boldsymbol{X}_2) = (a, b)$.

E2: For the 3D map, a period-doubling bifurcation generates a period-2 cycle ($m = 3$, $l = 2$), which is represented as $(\boldsymbol{X}_1, \boldsymbol{X}_2) = (a, b, a, b, a, b)$. Then, (a, b, a) and (b, a, b) form the period-2 cycle.

E3: For the 2D map, a period-3 cycle generated by a Hopf bifurcation ($m = 2$, $l = 3$) is represented as $(\boldsymbol{X}_1, \boldsymbol{X}_2, \boldsymbol{X}_3) = (a, b, c, a, b, c)$; (a, b), (c, a), and (b, c) form the period-3 cycle. For the case of $\alpha_1/\alpha_2 = 1$ (see Fig. 9), the solution with $b = c$ is observed, i.e., $(x_0, x_1, x_2) = (a, b, b)$.

E4: For the 3D map, a period-5 cycle generated by a Hopf bifurcation ($m = 3$, $l = 5$) is represented as $(\boldsymbol{X}_1, \boldsymbol{X}_2, \boldsymbol{X}_3, \boldsymbol{X}_4, \boldsymbol{X}_5) = (a, b, c, d, e, a, b, c, d, e, a, b, c, d, e)$; (a, b, c), (d, e, a), (b, c, d), (e, a, b), and (c, d, e) form the period-5 cycle. For the case of $\alpha_1/\alpha_2 = 1$ and $t_1/t_2 = 2/3$ [see Fig. 8(b)], the solution with $a = e$ and $b = d$ is observed, i.e., $(x_0, x_1, x_2, x_3, x_4) = (a, b, c, b, a)$.

E5: An exception to item **R2** that two fixed points coexist: for the 2D map, a pitchfork bifurcation generates a pair of fixed points ($m = 2$, $l = 1$), each of which is represented as either $\boldsymbol{X} = (a, b)$ or $\boldsymbol{X} = (b, a)$. The corresponding solution of the two-to-one map is written as $(x_0, x_1, x_2, x_3, \cdots) = (a, b, a, b, \cdots)$ or $(b, a, b, a \cdots)$.

Let us consider the correspondence of the solutions of the two-to-one map (9) or m-dimensional map (11) to those of the time-continuous nondispersive system (3). Remember that a single iteration of the two-to-one map (9) corresponds to the time interval t_2/m. For the nondispersive system (3), from item **A1** in Sect. 3.1, a solution excited by the first bifurcation at the relevant condition $t_{1R}/t_2 = n/m$ is a rectangular wave with the unit step width t_2/m and with period $T_f/m (= 2t_2/m)$, which is consistent with items **E2** and **E5**. We can also assume that a period-l cycle for the two-to-one map (9) corresponds to a piecewise-constant wave consisting of l steps.

Let us consider solutions for the dispersive system (1). From item **A1** in Sect. 3.1, a rounded rectangular wave whose period is approximated by T_f/m should be observed in a neighborhood of the relevant condition for the dispersive system if the cutoff angular frequency ω_{cut} ($\propto \gamma$) is higher than $m\omega_f$. If a stepwise wave consisting of l steps with period lt_2/m is a solution for an irrelevant condition $t_{1I}/t_2 = n/m$ of the nondispersive system, a rounded stepwise wave with a unit step width $\approx t_2/m$ and with period $\approx lt_2/m$ should be observed at the point $t_1 = t_{1I} + \Delta t_\gamma$. However, if $l > 2m$, such a rounded stepwise wave, except subharmonic waves generated by a period-doubling cascade, seems not to be allowed because a wave with period larger than T_f is suppressed by the effect of the long delay t_2 combined with the dispersion.

Let us consider how a solution with an irrational rotation number induced by a Hopf bifurcation for the m-dimensional map is transformed to that for the dispersive system. The

eigenvalues of the Hopf bifurcation are given by $\lambda_\pm = \exp \pm i\theta$ ($0 < \theta < \pi$), where $\theta_+/2\pi = \theta/2\pi$ and $\theta_-/2\pi = 1 - \theta/2\pi$ are rotation numbers. For the time-continuous system, they are interpreted as angular frequencies $\omega_\pm = \theta_\pm/t_2$ and $T_\pm = 2\pi t_2/\theta_\pm = \pi T_f/\theta_\pm$ because a single iteration of the m-dimensional map corresponds to the time interval t_2. At an irrelevant condition for NBP or BBP, $\theta_\pm = \pi \mp \epsilon$, where ϵ is a positive real number such that $0 < \epsilon < \pi/2$, and the period of the oscillation for the dispersive system is estimated as $T_\pm = \pi T_f \theta_\pm \approx T_f$ (see Figs.7 and 13), i.e., nearly the period of the fundamental wave. At an irrelevant condition for ABP, θ_- and $\theta_+ + 2\pi$ are close to 2π (see Fig. 16) and the period of the oscillation for the dispersive system is estimated as $T_- = \pi T_f/\theta_- \approx T_f/2$ or $T_+ = \pi T_f/(\theta_+ + 2\pi) \approx T_f/2$, i.e., nearly half the period of the fundamental wave.

5.2 Bifurcation diagrams in the NBP regime

To obtain a bifurcation diagram, we observe the change in oscillation with increasing μ at the rate $d\mu/dt = 4.2 \times 10^{-5}$. Figures 21(a) and 21(b) show bifurcation diagrams for $\alpha_1/\alpha_2 = 1/2$ and $\alpha_1/\alpha_2 = 1$, respectively. For the dispersive system, the relevant and irrelevant conditions slightly change as $t_1 \to t_1 + \Delta t_\gamma$ with $\Delta t_\gamma \approx -\gamma^{-1}(1 - t_1/t_2)$ [see Eq. (8)]. At $\gamma = 210$ and $t_2 = 1$, the relevant and irrelevant conditions $t_1 = 1/3$, $1/2$, and $2/3$ for the nondispersive system change to $t_1 = 104/315$, $209/420$, and $419/630$, respectively.

In Fig. 21, each bifurcation diagram is very similar to the corresponding diagram in Fig. 5. Bullets '•' are the first bifurcation points for the nondispersive system, i.e., the two-to-one map (9) with $t_1 = 1/3$, $1/2$, and $2/3$. The bifurcation points obtained numerically are delayed from those for the nondispersive system. This discrepancy is mainly attributed to a delayed response due to the weak instability of the fixed point just after the bifurcation.[20] Indeed, if the control parameter μ is kept constant after it reaches a point just above the bifurcation point for the nondispersive system, a gradually growing oscillation is observed for the dispersive system. Therefore, taking this ostensible discrepancy into account, the bifurcation points almost coincide with those of the nondispersive system. The insets show waves in the range $0.7 \le \mu \le 0.700252$, whose interval is three times as large as the wavelength of the fundamental wave in μ, i.e., $3T_f \frac{d\mu}{dt} = 2.52 \times 10^{-4}$.

In the NBP regime, $t_1 = 1/3 + \Delta t_\gamma$ is a relevant condition, at which a (rounded) rectangular wave with period $T \approx T_f/3$, i.e., the 3rd mode, is excited by the first bifurcation of the fixed point [see the red lines at $t_1 = 1/3 + \Delta t_\gamma$ in the insets of Figs. 21(a) and 21(b)]. This is predicted from items **A1** and **E2**.

The conditions $t_1 = 1/2 + \Delta t_\gamma$ and $t_1 = 2/3 + \Delta t_\gamma$ are irrelevant. For the 2D map (13) and

3D map (57), the first bifurcations of the fixed point are Hopf bifurcations, and are always delayed from that of the relevant condition. The same tendency is observed for the dispersive system. For the 2D and 3D maps with $\alpha_1/\alpha_2 = 1/2$, oscillations each with an irrational rotation number are excited by the first bifurcations [see Fig. 5(a)], and as counterparts in the dispersive system, sinusoidal-like waves are observed. At $t_1 = 2/3 + \Delta t_\gamma$, the period of the wave T is slightly shorter than T_f [see the green line at $t_1 = 2/3 + \Delta t_\gamma$ in the inset of Fig. 21(a)]. This is explained from the discussion in Sect. 5.1. That is, if the rotation angle θ_-, which is slightly larger than π, is chosen, the period of the wave is given as $T = \pi T_f/\theta_- \approx T_f$. However, at $t_1 = 1/2 + \Delta t_\gamma$, a wave with a period slightly longer than $T_f/3$, i.e., almost the 3rd harmonic, is observed (see the blue line at $t_1 = 1/2 + \Delta t_\gamma$ in the inset). It is explained that if θ_+ is replaced with $\theta_+ + 2\pi$ taking the arbitrariness in the phase by 2π into account, it gives the period $T \approx T_f/3$. In this case, the irrelevant condition seems to shift slightly toward the positive direction. Indeed, at $t_1/t_2 = 1046/2100$ ($> 1/2 + \Delta t_\gamma$), a wave with period slightly shorter than T_f is observed (see the thin black line in the inset). For the 2D map (13) and 3D map (57) with $\alpha_1/\alpha_2 = 1$, period-3 and period-5 cycles are observed, respectively [see Figs. 9 and 8(b)]. For the dispersive system at $t_1/t_2 = 1/2 + \Delta t_\gamma$, a period-3 stepwise wave with a unit step width $\approx t_2/2$ and with period $T \approx 3t_2/2$ is observed and its waveform is explained from items **R2** and **E3** [see the blue line at $t_1/t_2 = 1/2 + \Delta t_\gamma$ in the inset of Fig. 21(b)]. At $t_1/t_2 = 2/3 + \Delta t_\gamma$, a period-5 stepwise wave with a unit step width $\approx t_2/3$ and with period $T \approx 5t_2/3$ is observed and its waveform is explained from items **R2** and **E4** [see the green line at $t_1/t_2 = 2/3 + \Delta t_\gamma$ in the inset].

5.3 Bifurcation diagrams in the BBP regime at $\alpha_1/\alpha_2 = -1/2$

Figures 22(a) and 22(b) show bifurcation diagrams and representative waves in the insets for the relevant condition $t_1/t_2 = 2/3 + \Delta t_\gamma$ and the irrelevant condition at $t_1/t_2 = 1/2 + \Delta t_\gamma$, respectively. Each envelope of the bifurcation diagrams closely imitates that for the nondispersive system (see Figs.11 and 17).

At the relevant condition $t_1/t_2 = 2/3+\Delta t_\gamma$, as shown in the inset of Fig. 22(a), a rectangular wave with a unit step width $\approx t_2/3$ and with period $T \approx T_f/3$ is excited by the first bifurcation (see the red wave at $\mu \approx 0.8$), but, with increasing μ, it changes to a deformed rectangular wave at point b, which seems to be a superposition of a rectangular wave and a high-frequency wave with a small amplitude (see the blue wave at $\mu \approx 0.9$). At point b, twin circles with an irrational rotation number are observed for the nondispersive system [see Fig. 12(a)]. Thus, the wave of the dispersive system seems to be related to it. At point c, an irregular wave with

(a)

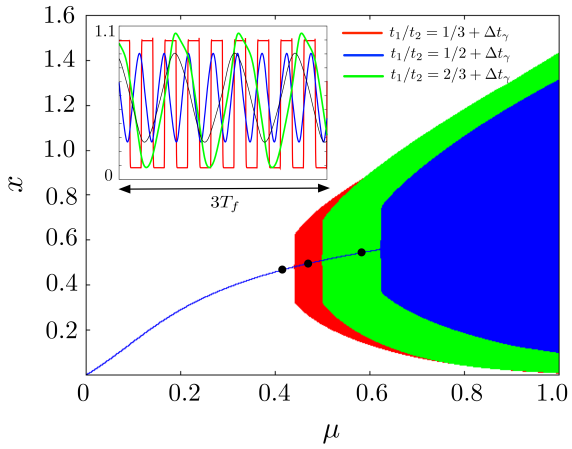

(b)

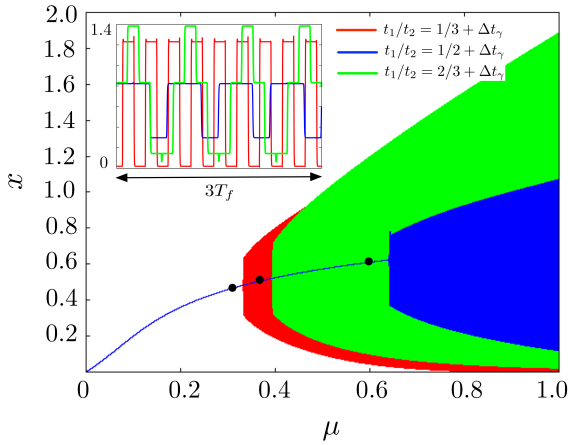

Fig. 21. (Color online) Bifurcation diagrams for the two-delay system (1) in the NBP regime at $\gamma = 210$, $t_2 = 1$, $\alpha_2 = 1$, $x_0 = 0.2$, and $\Delta t = 0.5$ when the control parameter μ is increased at the rate $d\mu/dt = 4.2 \times 10^{-5}$. The points denoted by the bullet '•' are the first bifurcation points of the fixed point x_c for the two-to-one map (9). (a) Oscillations at $\alpha_1/\alpha_2 = 1/2$. The inset shows waves in the range $0.7 \le \mu \le 0.700252$, which corresponds to the time interval $3T_f$. The colors (lightness in monochrome printing) of lines correspond to those of the bifurcation diagram except for the thin black line, which is a wave at $t_1/t_2 = 1046/2100$. (b) Oscillations at $\alpha_1/\alpha_2 = 1$. The inset shows the waves in the range $0.7 \le \mu \le 0.700252$, i.e., the time interval $3T_f$.

high-frequency components is observed (see the green wave at $\mu \approx 0.99$ in the inset) and corresponds to a chaotic attractor for the nondispersive system [see Fig. 12(b)].

The numerical result at the irrelevant condition $t_1/t_2 = 1/2 + \Delta t_\gamma$ is shown in Fig. 22(b). A sinusoidal-like wave (the red wave at $\mu \approx 0.9$ in the inset) is excited by the first bifurcation as a counterpart of the oscillation with an irrational rotation number for the nondispersive system at $t_1/t_2 = 1/2$ (see Fig. 17). The period of this wave is slightly larger than T_f. It means that the rotation angle θ_+, which is slightly less than π, is chosen. As shown by the blue wave

at $\mu \approx 0.99$ in the inset, it changes to a period-5 stepwise wave with a unit step width$\approx t_2/5$, which should correspond to one of the paired period-5 cycles for the nondispersive system. Finally it changes to a chaotic oscillation as the nondispersive system does (see the green wave at $\mu \approx 1.1$ in the inset).

(a)

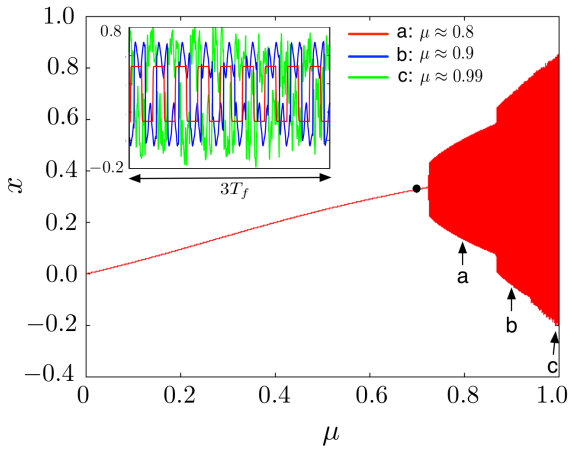

(b)

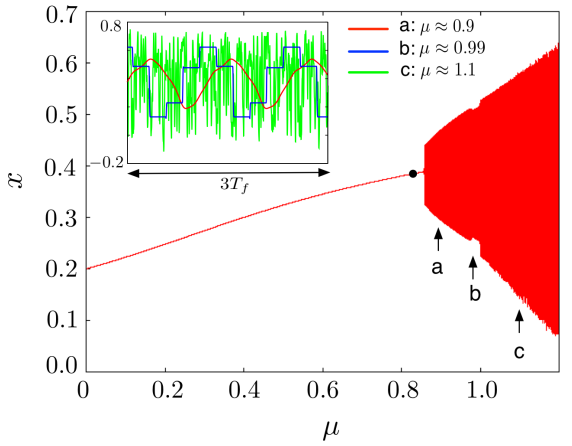

Fig. 22. (Color online) Bifurcation diagrams for the two-delay system (1) with $\alpha_1/\alpha_2 = -1/2$. The other parameters are the same as those in Fig. 21. The points denoted by the bullet '•' are the first bifurcation points of the fixed point x_c for the two-to-one map (9). The insets show waves observed near the points labeled 'a', 'b', and 'c'. (a) $t_1/t_2 = 2/3 + \Delta t_\gamma$. (b) $t_1/t_2 = 1/2 + \Delta t_\gamma$.

5.4 Bifurcation diagrams in the ABP regime at $\alpha_1/\alpha_2 = -0.9$

As shown in Figs. 23(a) and 24(a), there exist dominant attractors labeled 'D', 'D1', and 'D2', and subdominant attractors labeled 'S', which exactly correspond to those observed for the nondispersive system (see Figs. 14 and 18). First, we discuss the dominant attractors.

5.4.1 Dominant attractors

• Irrelevant condition $t_1/t_2 = 2/3 + \Delta t_\gamma$

Figure 23 shows the result of the irrelevant condition $t_1/t_2 = 2/3 + \Delta t_\gamma$. The first bifurcation of the fixed point generates an oscillation with period T slightly longer than $T_f/2$ [see the red wave at $\mu \approx 0.7$ in Fig. 23(b)] as discussed in Sect. 5.1. In Fig. 23(a), the attractor labeled 'D1' that is generated by the first bifurcation suddenly disappears at $\mu \approx 0.788$ owing to a subcritical-like bifurcation. This corresponds to the sudden disappearance of the attractor generated by the first bifurcation for the 3D map (57) (see Fig. 14). Thus, as shown in Fig. 23(a), motion is transferred to the outer attractor labeled 'D2', which extends downward until $\mu \approx 0.650$ and seems to continue upward without limit similarly to the outer attractor for the nondispersive system (see Fig. 14).

At $\mu \approx 0.8$, a period-12 stepwise wave with a unit step width $\approx t_2/3$ arises, although it is considerably deformed [see the blue wave at $\mu \approx 0.8$ in Fig. 23(b)]. For the 3D map, triplets of period-4 cycles are observed at $\mu \approx 0.787$ and change to forty-eight chaotic islands at $\mu \approx 0.8$ [see Fig. 15(a)]. Taking the delay of the response into account when μ is increased with a small rate $d\mu/dt = 4.2 \times 10^{-5}$, the oscillation at $\mu \approx 0.8$ should correspond to that for the nondispersive system at $\mu \approx 0.787$, and one of the triplets of period-4 cycles for the 3D map can be interpreted as the period-12 stepwise wave for the dispersive system. Note that item **R2** cannot be applied to this case because the assumption that there exists only one period-l cycle is not satisfied. The irregular oscillation observed at $\mu \approx 0.9$ [see the green wave at $\mu \approx 0.9$ in Fig. 23(b)] corresponds to a chaotic attractor for the 3D map [see Fig. 15(b)].

As shown in Fig. 23(c), irregular oscillations are observed at $\mu \approx 2$ and 2.9, although period-7 cycles are observed for the 3D map [see Fig. 15(c)]. From item **R2**, the two-to-one map (56) has period-7 cycles, and a period-7 stepwise wave should appear for the dispersive system. However, $l > 2m$ ($l = 7, m = 3$) and such a stepwise wave with period longer than T_f is suppressed (see the discussion in Sect.5.1).

• Relevant condition $t_1/t_2 = 1/2 + \Delta t_\gamma$

Figure 24 shows the result of the relevant condition $t_1/t_2 = 1/2 + \Delta t_\gamma$. In Fig. 24(a), the attractor labeled 'D' is generated by the first bifurcation. A period-2 stepwise wave with a unit step width $\approx t_2/2$ is generated by the first bifurcation of the fixed point [see the red wave at $\mu \approx 0.6$ in Fig. 24(b)]. From item **E5**, it corresponds to one of the paired fixed points generated by the pitchfork bifurcation for the 2D map (13) [see Fig. 19(a)]. At $\mu \approx 0.75$, a period-4

stepwise wave is observed [see the blue wave at $\mu \approx 0.75$ in Fig. 24(b)] and corresponds to one of the paired period-2 cycles for the 2D map, which are generated from the paired fixed points by the period-doubling bifurcation. At $\mu \approx 0.8$, a deformed period-8 stepwise wave is observed [see the green wave at $\mu \approx 0.8$ in Fig. 24(b)] and should correspond to one of the paired period-4 cycles in the period-doubling cascades for the 2D map. However the paired period-8 cycles are already created by the third period-doubling bifurcation at $\mu \approx 0.796$ for the 2D map. This discrepancy between the dispersive system and the 2D map is attributed to the delay of the response when μ is increased with a small but nonzero rate. The irregular oscillation observed at $\mu \approx 0.9$ [see the purple wave at $\mu \approx 0.9$ in Fig. 24(b)] corresponds to a chaotic attractor for the 2D map [see Fig. 19(b)]. As shown in Fig. 24(c), period-3 stepwise waves are observed at $\mu \approx 2$ and 2.9 and, from item **R2**, correspond to period-3 cycles for the 2D map [see Fig. 19(c)].

5.4.2 Subdominant attractors

First, we explain the method of obtaining subdominant attractors. For $\alpha_1/\alpha_2 = -0.9$, $x_c = 0.2$ and $f'(x_c) = 0$ at $\mu = 2$ from Eqs.(5) and (6) with $x_0 = 0.2$ and $\Delta x = 0.5$. Then, we start at $\mu = 2$ and $x = 0.2$, and either increase or decrease μ with the rate $|d\mu/dt| = 4.2 \times 10^{-5}$ until the subdominant attractor disappears and motion is transferred to the dominant attractor owing to a subcritical-like bifurcation.

In the upward process, the bifurcation of the fixed point is governed by BBP. The numerical result is shown in Fig. 25(a). At $t_1/t_2 = 2/3 + \Delta t_\gamma$, i.e., the relevant condition for BBP, a rectangular wave with period $T \approx T_f/3$ is excited by the bifurcation of the fixed point (see the green wave at $t_1/t_2 = 2/3 + \Delta t_\gamma$ in the inset) and it further changes in a similar way to that in Fig. 22(a) until it is transferred to the dominant attractor. At the irrelevant condition $t_1/t_2 = 1/2 + \Delta t_\gamma$, a wave with period slightly larger than T_f is excited by the bifurcation of the fixed point (see the blue wave at $t_1/t_2 = 1/2 + \Delta t_\gamma$ in the inset) and it further changes in a similar way to that in Fig. 22(b). Therefore, the upward processes at $t_1/t_2 = 2/3 + \Delta t_\gamma$ and $1/2 + \Delta t_\gamma$ are in the BBP regime and correspond to those for the 3D map (57) and the 2D map (13), respectively (see Figs.14 and 18).

In the downward process, the bifurcation of the fixed point is governed by ABP [see Fig. 25(b)]. At $t_1/t_2 = 1/2 + \Delta t_\gamma$, i.e., the relevant condition for ABP, a sinusoidal-like wave with period $T \approx T_f/2$ is excited by the bifurcation of the fixed point, but it gradually diverges with decreasing μ (see the blue wave at $t_1/t_2 = 1/2 + \Delta t_\gamma$ in the inset). This means that the bifurcation is subcritical and induces weak instability, which corresponds to the weak

instability of solutions in the same situation for the 2D map (13) (see Fig. 18). At the irrelevant condition $t_1/t_2 = 2/3 + \Delta t_\gamma$, a wave with period $T \approx T_f/2$ is excited by the bifurcation of the fixed point (see the green wave at $t_1/t_2 = 2/3 + \Delta t_\gamma$ in the inset) and closely reflects the characteristic of solutions in the same situation for the 3D map (57) (see Fig. 14). Therefore, the downward processes are in the ABP regime.

It is numerically confirmed that the subdominant attractors exist in almost all the range $0 < t_1/t_2 < 1$. Furthermore, we can check the mode selection rules for the upward and downward processes starting at $\mu = 2$ and $x = 0.2$. Figures 26(a) and 26(b) show the normalized frequency ω/ω_f of the first excited mode and the bifurcation points for the upward and downward processes, respectively, as functions of t_1/t_2. As shown in Fig. 26(a), the mode selection rules in the BBP and ABP regimes are observed for the upward and downward processes and are almost the same as those observed for the dominant attractors in the BBP and ABP regimes, respectively [see Figs. 2(b) and 2(c)]. As shown in Fig. 26(b), at the irrelevant conditions, e.g., $t_1/t_2 \approx 1/2$, $1/3$, and $1/4$ in the BBP regime, and $t_1/t_2 \approx 1/3$, $2/3$, and $1/5$ in the ABP regime, the bifurcations are relatively delayed compared with those for the relevant conditions, e.g., $t_1/t_2 \approx 2/3$ in the BBP regime, and $t_1/t_2 \approx 1/2$ and $1/4$ in the ABP regime, and the fixed point x_c is stable between the upper blue line and lower red line.

6. Discussion

In this paper, we explored how the mode selection rules and bifurcation diagrams for the two-delay system (1) with the function $f(x)$ given by (2) and with a finite γ, i.e., the dispersive system, are controlled by the multidimensional maps of the nondispersive system in the limit of $\gamma \to \infty$. At each of the relevant and irrelevant conditions for the nondispersive system, the rate of delay times t_1/t_2 is a rational number with $t_1/t_2 = n/m$ and each nondispersive system is transformed to a m-dimensional map. We focused on three simple cases, $t_1/t_2 = 1/3$, $1/2$, and $2/3$, which exchange the roles of the relevant and irrelevant conditions for the normal bifurcation process (NBP), the boosted bifurcation process (BBP), and the anomalous bifurcation process (ABP) (see Table I).

The mode selection rule is determined by the mechanism of the first bifurcation of the fixed point x_c. In terms of the multidimensional maps of the nondispersive system, either a pitchfork bifurcation with $\lambda = 1$ or a period-doubling bifurcation with $\lambda = -1$ occurs for the relevant condition, while a Hopf bifurcation is observed for the irrelevant condition. Technically, period-doubling bifurcations with $\lambda = -1$ occur for the relevant conditions in the NBP and BBP regimes and a pitchfork bifurcation with $\lambda = 1$ is observed for the relevant con-

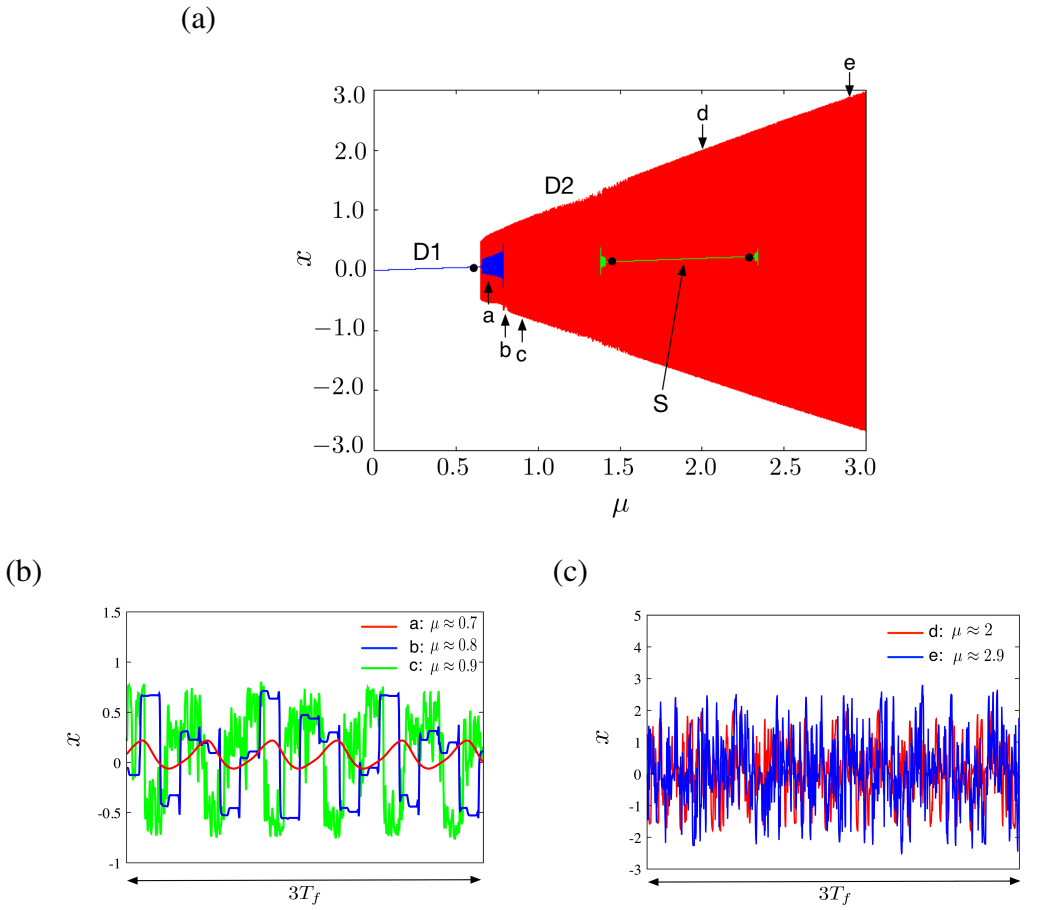

Fig. 23. (Color online) Bifurcation diagram and waves generated by bifurcations for the two-delay system (1) with $\alpha_1/\alpha_2 = -0.9$ and $t_1/t_2 = 2/3 + \Delta t_\gamma$. The other parameters are the same as those in Fig. 21. (a) Bifurcation diagram: the oscillation on the attractor generated by the first bifurcation (blue), that on the outer attractor (red), and that on the subdominant attractor (green) are labeled 'D1', 'D2', and 'S', respectively. The points denoted by the bullet '•' are the bifurcation points of the fixed point x_c for the two-to-one map (9). (b) Waves near the points labeled 'a', 'b', and 'c' in the bifurcation diagram. (c) Waves near the points labeled 'd' and 'e'.

dition in the ABP regime. These reflect the fact that the first bifurcation occurs in the range $f'(x_c) < 0$ for NBP and BBP and in the range $f'(x_c) > 0$ for ABP. The first bifurcation point for the relevant condition is determined by α_1 if α_2 is fixed, namely, $\mu(|\alpha_1| + \alpha_2)f'(x_c) = -1$ for NBP and BBP and $\mu(|\alpha_1| + \alpha_2)f'(x_c) = 1$ for ABP.[20] If $|\eta|$ $(= |\mu f'(x_c)|)$ is a monotonically increasing function of μ in a neighborhood of the first bifurcation, the first bifurcation for an irrelevant condition always arises at a larger value of μ than that for the relevant condition. Namely, $|\eta|$ at the first bifurcation point is larger for an irrelevant condition than for the relevant condition.[18,20]

The properties of the first bifurcations of the fixed point mentioned above almost hold for the dispersive system. The bifurcation points for the relevant and irrelevant conditions

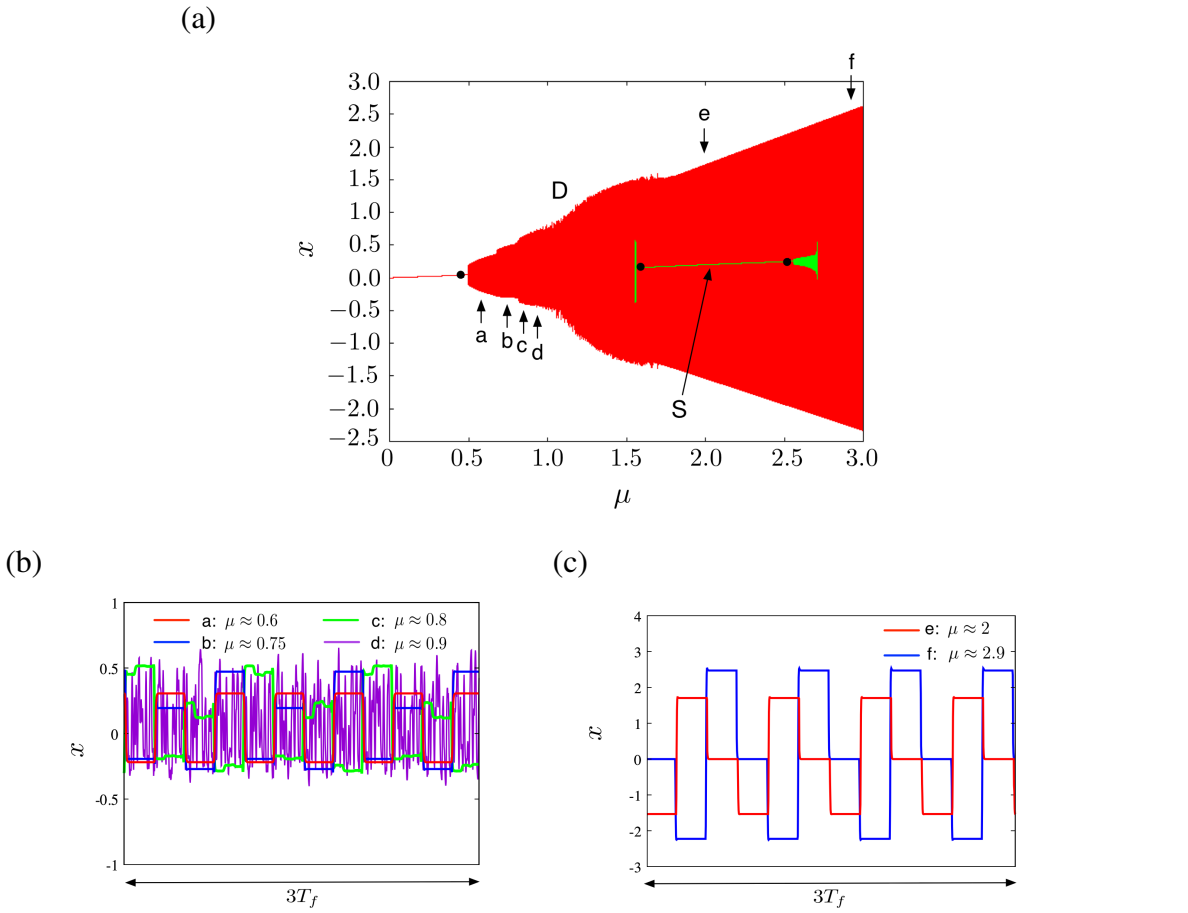

Fig. 24. (Color online) Bifurcation diagram and waves generated by bifurcations for the two-delay system (1) with $\alpha_1/\alpha_2 = -0.9$ and $t_1/t_2 = 1/2 + \Delta t_\gamma$. The other parameters are the same as those in Fig. 21. (a) Bifurcation diagram: the oscillation on the dominant attractor (red) and that on the subdominant attractor (green) are labeled 'D' and 'S', respectively. The points denoted by the bullet '•' are the bifurcation points of the fixed point x_c for the two-to-one map (9). (b) Waves near the points labeled 'a', 'b' , 'c', and 'd' in the bifurcation diagram. (c) Waves near the points labeled 'e' and 'f'.

are well approximated by those for the nondispersive system if γ is sufficiently large. As schematically shown in Fig. 4, rounded rectangular waves, each with period $T \approx T_f/m$, are observed in a neighborhood of a relevant condition if m is sufficiently smaller than γ. In the limit of $\gamma \to \infty$, the rounded rectangular waves converge to the rectangular wave with period $T = t_f/m$ at the relevant condition of the nondispersive system. On the other hand, in a neighborhood of an irrelevant condition, twin peaks consisting of higher-order harmonics, i.e., the tower structure, are observed. At the center of the twin peaks, i.e., the irrelevant condition, $|\eta|$ at the first bifurcation takes almost the same value as that for the nondispersive system, and a lower-order mode wave, whose period T can be estimated from the eigenvalues λ at the first bifurcation of the m-dimensional map, is observed.

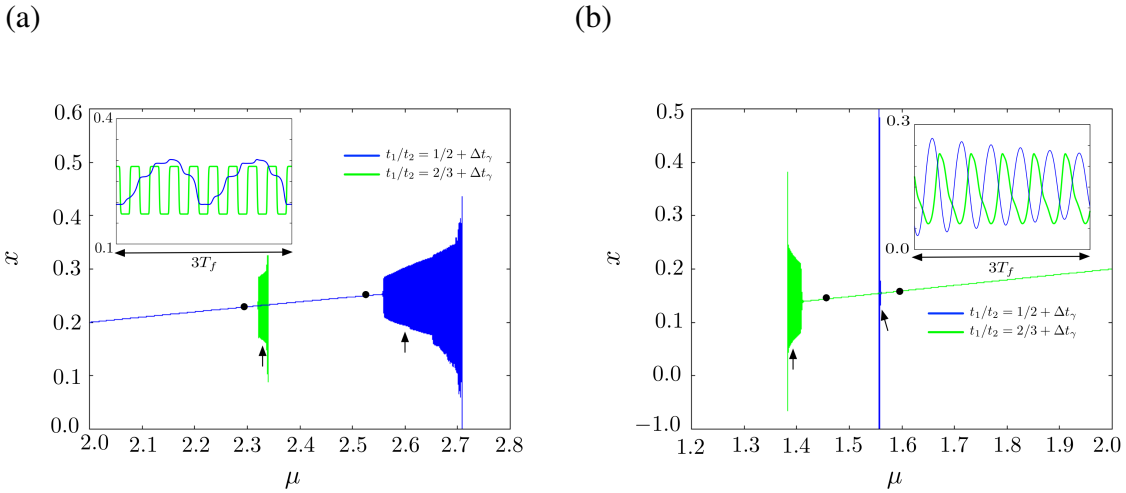

Fig. 25. (Color online) Bifurcation diagrams and waves generated by bifurcations of the subdominant attractors in Figs. 23 and 24. The points denoted by the bullet '•' are the bifurcation points of the fixed point x_c for the two-to-one map (9). (a) Bifurcation diagrams observed with increasing μ from $\mu = 2$. The inset shows waves near the points indicated by the arrows. (b) Bifurcation diagrams are observed with decreasing μ from $\mu = 2$. The inset shows waves near the points indicated by the arrows.

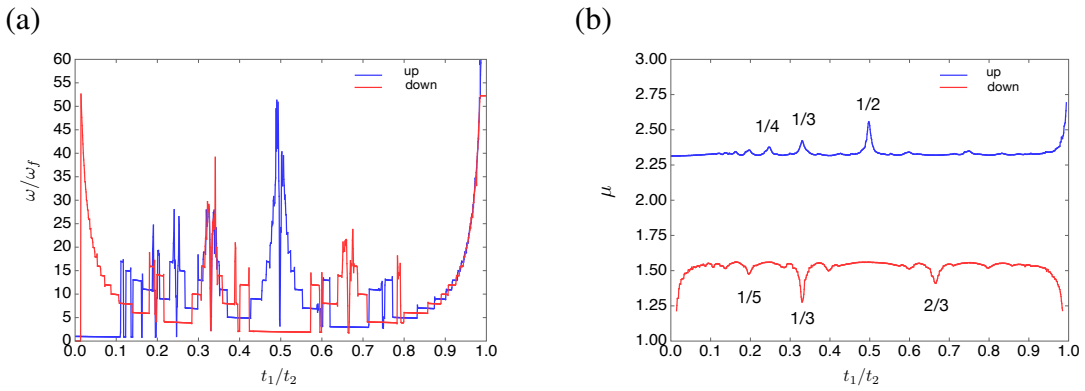

Fig. 26. (Color online) Normalized frequency ω/ω_f of the first excited mode and the bifurcation point of the fixed point on the subdominant attractor as functions of t_1/t_2 when μ is increased or decreased from $\mu = 2$ and $x = 0.2$. (a) Normalized frequencies ω/ω_f. (b) Bifurcation points of the fixed point.

As a result, the difference in the mechanism of the first bifurcation between the relevant and irrelevant conditions is clarified in terms of the multidimensional maps. The waves excited by the first bifurcation for the relevant and irrelevant conditions of the dispersive system are predicted from the analysis of the multidimensional maps. However, the analysis based on the multidimensional maps is not suitable for the study of the mode selection rule in the whole range of t_1/t_2. This is because the multidimensional maps defined point by point for rational numbers are different from each other, making it practically impossible to apply the

analysis based on the multidimensional maps to the study of the mode selection rule for the dispersive system, taking the effect of the cutoff frequency ω_{cut}, which is roughly estimated as $\omega_{cut} \propto \gamma$,[9,19] into account. Practically, the linear mode stability analysis studied in the previous works[6,9,18,20] is suitable for this purpose.

The most noteworthy result of this paper is that the analysis of the multidimensional maps gives an important perspective on the study of the bifurcation of attractors in a physically important range of the control parameter μ for the dispersive system. Indeed, the global structure of transitions among attractors is well captured by the multidimensional maps. For regular attractors including but not limited to the attractor excited by the first bifurcation except a few cases, waveforms for the dispersive system are interpreted from the solutions of the multidimensional maps. An example of an exceptional case is a solution with period l larger than $2m$. As counterparts of such exceptional cases and chaotic solutions, irregular oscillations with high-frequency components are mostly observed for the dispersive system.

The most important fact revealed from the study of the multidimensional maps is the existence of subdominant attractors in the ABP regime. The restabilization of the fixed point in the range $f'(x_c) > 0$ after the first bifurcation induces the subdominant attractor, whereas the dominant attractor exists independently. Note that for an irrelevant condition of ABP, the attractor excited by the first bifurcation of the fixed point subsequently disappears owing to a subcritical-like bifurcation, and motion is transferred to the outer attractor, which is regarded as the dominant attractor. The restabilized fixed point bifurcates again in the range $f'(x_c) < 0$; thus, this bifurcation is governed by BBP and the mode selection in the BBP regime is observed. The subdominant attractors exist in limited ranges of μ due to subcritical-like bifurcations. For the dispersive system, the subdominant attractors are generated and exist in the same way. Furthermore, the existence of the subdominant attractors is not restricted to the three simple cases, $t_1/t_2 = 1/3$, $1/2$, and $2/3$. Namely, it is numerically confirmed for the dispersive system that subdominant attractors exist in almost all the range of $0 < t_1/t_2 < 1$, and oscillations excited at upper and lower bifurcation points of the fixed point x_c on the subdominant attractor obey the mode selection rules of BBP and ABP, respectively.

As a result, for the simple cases studied in this paper, the properties of the first bifurcations, the mode selection rules, and the global structure of transitions among attractors in the NBP, BBP, and ABP regimes are approximately predicted from the analysis of the multidimensional maps of the nondispersive system. It is expected for all the relevant and irrelevant conditions that if excited modes are less than the cutoff, bifurcation phenomena can be predicted from the study of the multidimensional maps, although it is practically impossible to

handle all the multidimensional maps. As pointed out in the previous work,[20] the appearance of attractors in the ABP regime depends on the characteristic of the function $f(x)$ included in the two-delay system (1). For example, the dominant attractor in the ABP regime disappears for the two-delay system including the logistic map due to the interference between the two fixed points in the range $f'(x) > 0$. Even in this case, the subdominant attractor whose bifurcation is governed by BBP still survives. We will report the details of this two-delay system in future work.

Acknowledgment

The present work was supported by a Grant-in-Aid for Scientific Research (C) No. 16K05477 from the Japan Society for the Promotion of Science (JSPS) and by "Joint Usage/Research Center for Interdisciplinary Large-Scale Information Infrastructures" in Japan (Project ID: jh180007-MDH).

Appendix: Solutions of a cubic equation

Let us consider the cubic equation

$$x^3 + a_1 x^2 + a_2 x + a_3 = 0. \tag{A·1}$$

The roots of this equation are given as follows. We introduce coefficients Q, R, and D defined by

$$\begin{aligned} Q &= \frac{3a_2 - a_1^2}{9}, \\ R &= \frac{9a_1a_2 - 27a_3 - 2a_1^3}{54}, \\ D &= Q^3 + R^2, \end{aligned} \tag{A·2}$$

and define coefficients S and T as

$$S = \sqrt[3]{R + \sqrt{D}}, \tag{A·3}$$

$$T = \sqrt[3]{R - \sqrt{D}}. \tag{A·4}$$

Depending on the value of D, the roots are categorized into three cases:

i) $D > 0$: one real root and two nonreal complex conjugate roots.

ii) $D = 0$: a multiple root and all of its roots are real.

iii) $D < 0$: three distinct real roots.

For $D \geq 0$, the roots are given as

$$x_1 = S + T - \frac{1}{3}a_1, \tag{A·5}$$

$$x_2 = -\frac{1}{2}(S + T) - \frac{1}{3}a_1 + i\frac{\sqrt{3}}{2}(S - T), \tag{A·6}$$

$$x_2 = -\frac{1}{2}(S + T) - \frac{1}{3}a_1 - i\frac{\sqrt{3}}{2}(S - T), \tag{A·7}$$

and for $D < 0$, they are given as

$$x_1 = 2\sqrt{-Q}\cos\left(\frac{\theta}{3}\right) - \frac{1}{3}a_1, \tag{A·8}$$

$$x_2 = 2\sqrt{-Q}\cos\left(\frac{\theta}{3} + \frac{2\pi}{3}\right) - \frac{1}{3}a_1, \tag{A·9}$$

$$x_2 = 2\sqrt{-Q}\cos\left(\frac{\theta}{3} + \frac{4\pi}{3}\right) - \frac{1}{3}a_1, \tag{A·10}$$

where $\cos\theta = R/\sqrt{-Q^3}$.

References

1) L. Dugard and E. I. Verriest (eds.), *Stability and Control of Time-Delay Systems* (Springer-Verlag, London, 1998).

2) J.-P. Richard, Automatica **39**, 1667 (2003).

3) K. Gu, V. L. Kharitonov, and J. Chen, *Stability of Time-Delay Systems* (Birkhäuser, Boston, 2003).

4) M. Lakshmanan and D. V. Senthilkumar, *Dynamics of Nonlinear Time-Delay Systems* (Springer-Verlag, Berlin, 2010).

5) D. Müller, A. Otto, and G. Radons, Phys. Rev. Lett. **120**, 084102 (2018).

6) K. Ikeda and M. Mizuno, Phys. Rev. Lett. **53**, 1340 (1984); M. Mizuno and K. Ikeda, Physica D **36**, 327 (1989).

7) H. J. Zhang and J. H. Dai, Opt. Lett. **11**, 245 (1986); H. J. Zhang, J. H. Dai, T. Y. Wang, F. L. Zhang, G. Xu, and S. P. Yang, in *Directions in Chaos*, ed. H. Bai-Lin (World Scientific, Singapore, 1988) Vol. 2, p. 47.

8) C. Marriott, R. Vallée, and C. Delisle, Phys. Rev. A **40**, 3420 (1989).

9) C. Grotta-Ragazzo and C. P. Malta, J. Dyn. Differ. Equat. **4**, 617 (1992).

10) A. Hohl, A. Gavrielides, T. Erneux, and V. Kovanis, Phys. Rev. A **59**, 3941 (1999).

11) J. K. Hale and W. Huang, J. Math. Anal. Appl. **178**, 344 (1993).

12) J. Bélair and S. A. Campbell, SIAM J. Appl. Math. **54**, 1402 (1994).

13) X. Li, S. Ruan, and J. Wei, J. Math. Anal. Appl. **236**, 254 (1999).

14) S. Ruan and J. Wei, Dynam. Contin. Discrete Impuls. Systems A: Math. Anal. **10**, 863 (2003).

15) J. C. Bastos de Figueiredo, L. Diambra, L. Glass, and C. P. Malta, Phys. Rev. E **65**, 051905 (2002).

16) H.-J. Wünsche, S. Bauer, J. Kreissl, O. Ushakov, N. Korneyev, F. Henneberger, E. Wille, H. Erzgraber, M. Peil, W. Elsäßer, and I. Fischer, Phys. Rev. Lett. **94**, 163901 (2005).

17) X. F. Liao, Chaos Solitons & Fractals **23**, 857 (2005).

18) K. Takahashi, K. Goya, and S. Goya, J. Phys. Soc. Jpn. **83**, 124003 (2014).

19) K. Takahashi and T. Kobayashi, J. Phys. Soc. Jpn. **86**, 124005 (2017).

20) K. Takahashi and T. Kobayashi, J. Phys. Soc. Jpn. **87**, 044001 (2018).

21) R. T. Schumacher, Acustica **48**, 71 (1981).

22) M. E. McIntyre, R. T. Schumacher, and J. Woodhouse, J. Acoust. Soc. Am. **74**, 1325 (1983).

23) N. H. Fletcher and T. D. Rossing, *The Physics of Musical Instruments* (Springer-Verlag, New York, 1998) 2nd ed.

24) J. Guckenheimer and P. Holmes, *Nonlinear Oscillations, Dynamical Systems, and Bifurcations of Vector Fields* (Springer-Verlag, New York, 1983).

25) P. Bergé, Y. Pomeaú, and Ch. Vidal, *L'Ordre dans le Chaos*, (Hermann, Paris, 1984).